https://doi.org/10.5194/tc-2021-376
Preprint. Discussion started: 11 March 2022

The Cryosphere Discussions

Sublimation of frozen CsCl solutions in ESEM: determining the number and size of salt particles relevant to sea-salt aerosols

Ľubica Vetráková[1], Vilém Neděla[1], Jiří Runštuk[1], Xin Yang[2], Dominik Heger[3]

[1]Environmental Electron Microscopy Group, Institute of Scientific Instruments of the Czech Academy of Sciences, Brno, Czech Republic
[2]British Antarctic Survey, Natural Environment Research Council, Cambridge, UK
[3]Department of Chemistry, Faculty of Science, Masaryk University, Brno, Czech Republic
Correspondence to: Ľubica Vetráková (vetrakova@isibrno.cz) and Dominik Heger (hegerd@chemi.muni.cz)

Abstract. We identified the factors that, during the sublimation of a frozen CsCl solution, are important in generating fine salt particles as a possible source of salt aerosol. The number, size, and structure of the particles that remain after ice sublimation were investigated with respect to the concentration of the salt in the sample, the freezing method, and the sublimation temperature. The last-named aspect is evidently of primary importance for the preference of fine salt crystals over a large compact piece of salt. Independently of the concentration and freezing method tested, the sublimation of the frozen samples above the eutectic temperature (T_{eu}) yielded a large compact piece of salt, namely, an improbable source of aerosol particles. Small salt particles that might be a source of atmospheric aerosols were formed predominantly at the temperatures below T_{eu}, and their structures strongly depended on the concentration of the salt. For example, the sublimation of those samples that exhibited less than 8 psu (0.05 M) often produced small aerosolizable isolated particles readily able to be windblown. Conversely, the sublimation of 78 psu (0.5 M) samples led to the formation of relatively stable and largely interconnected salt structures. Presumably, our findings have important implications because the formed salt particles may assume the role of cloud condensation nuclei and ice-nucleating particles, affect polar atmospheric radiative forcing, and facilitate heterogeneous atmospheric chemistry.

1 Introduction

Periods of low tropospheric ozone concentrations (e.g., < 10 ppbv) in springtime were repeatedly observed in the polar tropospheric boundary layer (Barrie et al., 1988; Bottenheim et al., 2002; Richter et al., 1998). These ozone depletion events are attributed to the inorganic halogens in the polar atmosphere (Abbatt et al., 2012; Richter et al., 1998). Bromine radicals destroy ozone very efficiently; moreover, the number of reactive gaseous bromine can increase markedly during "bromine explosions", in which every Br atom of a gaseous HOBr molecule can cause an extra bromide release from saline sea salt aerosol or other salty particles (Kaleschke et al., 2004). Thus, all saline crystals in sea ice zones are potential sources of reactive bromine: the proposed candidates include frost flowers (Kaleschke et al., 2004), first-year sea ice (Simpson et al., 2007), sea salt aerosol (SSA) from blowing snow (Frey et al., 2020; Yang et al., 2008, 2019), SSA from open leads (Peterson et al., 2017),

https://doi.org/10.5194/tc-2021-376
Preprint. Discussion started: 11 March 2022


The Cryosphere Discussions

and the photochemistry within snowpack (Pratt et al., 2013). However, the exact sources of bromine in polar spring are still disputed (Abbatt et al., 2012).

Chemical analyses of SSAs in inland Antarctica show that the aerosols are sulphate-depleted relative to sodium, which points to a sea-ice source of the SSA (Jourdain et al., 2008; Legrand et al., 2017; Rankin and Wolff, 2003; Wagenbach et al., 1998). The suggested mechanism of the sulphate-depletion of the SSA is mirabilite ($Na_2SO_4.10H_2O$) precipitation from brine below −6.4°C (Butler et al., 2016), a fractionation not plausible in sea spray particles generated directly from open oceans. The windblown snow particles of relatively low salinity were suggested to be an efficient source of the SSA (Yang et al., 2008, 2019). The proposed blowing snow mechanism relating to SSA production was supported by the Antarctic Weddell Sea data (Frey et al., 2020). Previously, highly saline frost flowers on thin sea ice were also regarded as a significant source of the SSA (Kaleschke et al., 2004; Rankin and Wolff, 2003; Wolff et al., 2003); this was contradicted by both the wind tunnel experiment (Roscoe et al., 2011) and the *in situ* sublimation of frost flowers in an environmental scanning microscope (ESEM) (Yang et al., 2017). However, these two laboratory studies were performed in a relatively warm temperature range, between -5 to -18 °C; these values are above the eutectic temperature, T_{eu} = −21°C, of a NaCl solution (Rodebush, 1918). We are not aware of any laboratory research on the formation of the SSA at temperatures below T_{eu}, which often occur in polar regions in winter and early spring; moreover, most of the sea ice is covered by saline ice crystals, including either high salinity formations such as frost flowers and the basal part of a snowpack or low salinity ices comprising the snow at the surface layer of a snowpack and on thick multiyear sea ice. The investigation of the impact exerted by the temperature and saline concentration on SSA formation is critical in understanding the implications to polar atmospheric chemistry and climate. This is because SSAs not only are a reservoir of various chemical compounds but also function as cloud condensation nuclei (e.g. O'Dowd et al., 1999) or even ice nucleating particles (DeMott et al., 2016; Wise et al., 2012).

In this study, we utilize an ESEM to visualize the process of ice sublimation *in-situ* as well as the structures of the CsCl salt particles formed upon the sublimation. We inspect the potential of the frozen solutions to generate fine salt particles that may become a source of salt aerosol when airborne. The number, size, and structure of those salt particles that remain after ice sublimation were analyzed as the function of the salt concentration in the sample, the freezing method, and the sublimation temperature. Similarly, the effect of liquid sample evaporation slightly above the freezing point was inspected. This article follows on our previous paper in which the morphologies of salty frozen solutions were detailed (Vetráková et al., 2019).

2 Methods

2.1 Description of the ESEM

The microscopic images were recorded using a non-commercial ESEM AQUASEM II constructed from a Tescan VEGA SEM at the Institute of Scientific Instruments of the Czech Academy of Sciences (Neděla, 2007). Compared to a conventional SEM, the ESEM does not require high vacuum conditions in the specimen chamber. The ESEM is suitable for the direct imaging of wet, electrically non-conductive and electron beam-sensitive samples (Michaloudi et al., 2018) at chamber pressures up to

https://doi.org/10.5194/tc-2021-376
Preprint. Discussion started: 11 March 2022

2,000 Pa; the samples do not require conductive coating (Schenkmayerová et al., 2014). Moreover, the device allows in-situ observation under dynamically changing environmental conditions (Neděla et al., 2020). The samples are placed on the silicon pad of a Peltier cooling stage, which can reach temperatures down to −27 °C; this ESEM facilitates the imaging of frozen samples. The ambient pressure inside the specimen chamber was maintained at 500 Pa; the gaseous environment comprised mostly blown-in air, although a small amount of water vapour was present too due to ice sublimation. The electron beam energy to enable the imaging amounted to 20 keV. The low beam current (100 pA) and short dwell time (14 µs) minimise the radiation damage and local heating of frozen samples. The YAG:Ce^{3+} scintillation detector of backscattered electrons (BSE) is sensitive to signal from atoms with a large atomic number (Neděla et al., 2018); therefore, very good material contrast between the ice and the CsCl salt is obtained. In the images, both the CsCl crystals and the brine are represented in white, the ice is usually black, and the silicon surface of the cooling stage is grey. The reasons to use CsCl as a proxy of a sea salt are further discussed in section 4.

2.2 Freezing and sublimation

CsCl solutions with the concentrations of 0.005, 0.05, and 0.5 M (which approximates to 0.084, 0.83, and 7.8 wt%, or 0.84, 8.3, and 78 psu, respectively) were prepared via dissolving appropriate amounts of CsCl in MilliQ H_2O. The droplets with a diameter of ~ 4 mm were frozen at atmospheric pressure via three distinct methods:

(I) Spontaneous freezing of a droplet without seeding. The droplet was deposited onto the cooling stage of the ESEM. The temperature of the cooling stage was gradually lowered from room temperature (about 23 °C) down to the desired temperature at a cooling rate of ~ 0.5 °C/s; the sample froze spontaneously at −10 to −12 °C in the replicate experiments. Within this article, the samples are referred to as *non-seeded*.

(II) Controlled ice nucleation (seeding). The droplet was placed onto the cooling stage of the ESEM; subsequently, the stage was cooled down to −3 °C and, after the thermal equilibration, several small ice crystals were added to the edge of the sample to initiate the nucleation process. In the text, these samples are referred to as *seeded*.

(III) Freezing in liquid nitrogen (LN). A droplet of the sample was deposited on a piece of aluminium foil and immersed into the LN. The foil was used to ensure a flat bottom of the sample, guaranteeing a better thermal contact with the cooling stage of the ESEM. Then, the frozen sample was transferred onto the stage. Within the article, these samples are denoted as *LN-frozen*. In some of the experiments, small frozen spheres (a diameter of approx. 100 to 200 µm) were prepared (by spraying a solution into the LN) to evaluate the effect of the sample size.

Subsequently, the frozen samples were held at either −20 or −25 °C; the specimen chamber of the ESEM was closed and evacuated to 500 Pa. The chosen temperatures allow us to observe the differences in the sublimation above and below the T_{eu}, whose literature value ranges from −24.83 to −22.3 °C (Chen et al., 2005; Cohen-Adad and Lorimer, 1991; Dubois et al., 1993; Fujiwara and Nishimoto, 1998; Gao et al., 2017; Monnin and Dubois, 1999).

The freezing methods I and II are identical with those described in our previous paper (Vetráková et al., 2019), where the freezing rates were estimated to be (154 ± 13) mm s^{-1} in the non-seeded sample (method I) and ~ 0.2 mm s^{-1} in the seeded one (method II). The rate of the LN freezing (method III) was not determined. Apart from the freezing rate, the three freezing

https://doi.org/10.5194/tc-2021-376
Preprint. Discussion started: 11 March 2022

methods differ in the direction of freezing (a vector perpendicular to the progressing freezing front). Estimated directions incident to these freezing methods are outlined in Figure 1.

2.3 Evaporation

Droplets (~ 4 mm in diameter) of the liquid 0.005 and 0.05 M CsCl solutions were evaporated in the evacuated specimen chamber of the ESEM at the ambient air pressure of 650 Pa and the temperature of 2 °C.

3 Results

This paper describes the ice sublimation process above and below the T_{eu} and the morphology of the resulting residua of the non-seeded, seeded, and LN-frozen samples. The outcomes are compared to the residua after the evaporation of the salty water.

3.1 Sublimation above the T_{eu}

When the temperature during the sublimation reached −20 °C, which is above the T_{eu}, the CsCl brine was still in the liquid state; no salt crystals were observed on the surface of the ice (Figure S1a, c, e). The liquid brine accumulated at the edge of the sample on the cooling stage. As the sublimation proceeded, the diameter of the sample decreased, and the brine slowly shifted towards the retreating sample edge. At some point, the brine at the edge crystallized. The frozen sample continued reducing its size due to the sublimation, and soon the edge was separated from the crystallized brine. New liquid brine kept leaking out of the sample, and the situation recurred incessantly. The crystallization sequence at the edge is illustrated in Figure 2. The amount of the crystallized brine diminished progressively towards the centre of the sublimated sample because of the preceding drainage (Figures 3-5). After the sublimation, the crystalline CsCl was arranged in the form of concentric circles (Figure 6). The salt rings were usually thick and compact close to the periphery, but they became thinner towards the centre and, especially in the samples with the lowest salt concentration, even small isolated particles occurred at the very centre of the samples (Figure 3). This pattern was observed for the seeded and non-seeded samples in all of the concentrations (Figures 3-5, left and middle columns) and in the 0.005 M LN-frozen samples (Figure 3c).

In addition to the similarities in the output, the 0.05 and 0.5 M LN-frozen samples exhibited some differences (Figures 4-5, right columns). As in the previous cases, the liquid brine accumulated at the edge of the sample and, at a certain point, started to crystallize. However, such crystallization at the edge initialized the same process all over the surface of the frozen sample, and a fibrous, shell-like structure was formed on the surface. Despite its delicate appearance, the structure retained its shape even when the ice had completely sublimated.

Above the T_{eu}, the brine leaked out of the sample and the salt crystallized directly on the cooling stage; therefore, the crystallized salt was pinned to the surface of the cooling stage. Surprisingly, a number of small salt crystals occurred also far beyond the original perimeter of the frozen sample, where no bulk brine had apparently reached (see, e.g., Figures 4d, 4e, 5f,

https://doi.org/10.5194/tc-2021-376
Preprint. Discussion started: 11 March 2022

5i). Evidently, a precursor nanofilm (De Gennes, 1985) of the liquid brine (which could not be detected with the ESEM) had spread over the silicon surface to these remote locations, and, after the evaporation of water from the brine, the small salt crystals emerged (Qazi et al., 2019). A similar behaviour characterizes the non-seeded and seeded samples below the T_{eu}, as presented in chapter 3.2.5. In the LN-frozen samples, we detected these small, strayed crystals only at −20 °C (Figure 5 f, i); the brine has spread from the frozen samples, as it is liquid at this temperature above the T_{eu}.

3.2 Sublimation below the T_{eu}

For the sublimation to proceed below the T_{eu}, the temperature in our experiments was set to −25 °C. Although the temperature of the surface may slightly deviate from that of the cooling stage, solidified CsCl brine was visibly present on the surfaces of the frozen samples under the pre-set conditions in all of the concentrations and freezing methods. In a few replicates, however, the surface brine was still liquid at the temperature; these results are not included in the article. We estimated the sample temperature with a Pt1000 attached to the silicon pad to obtain a temperature 2 °C higher than the pre-set one. This temperature range corresponds roughly to the uncertainty on the CsCl eutectic point.

3.2.1 Concentration of 0.005 M

The sublimation residua of the 0.005 M CsCl are displayed in Figure 7, and they appear to be largely similar between the non-seeded and the seeded samples. Three types of residual salt structures were observed: 1. A flat rim at the location of the circumference of the frozen sample (Figure 7a, c); this rim supposedly formed from the brine that had leaked to the sample's edge before the T_{eu} had been reached during the freezing processes. This formation mechanism is supported by the fact that, if the temperature temporarily rises above the T_{eu} (and the brine liquifies) and then drops again, the salt rim becomes wider (analogous situation is shown in Figure S2). During these processes, surplus liquid brine was observed to leak to the edge of the sample. 2. Fine salt particles that appeared from beneath the samples and remained lying on the stage (Figures 7a, c, d) as the samples were sublimating; typically, their widths and lengths were approximately 1 µm and several micrometres, respectively. In the seeded sample, the microparticles were often arranged in straight lines (Figure 7c), while a random arrangement dominated in the non-seeded sample (Figure 7a). We processed the micrographs by using Mountains® software (Digital Surf) and estimated the abundance of the fine salt particles on the pad (Text S1); approximately 3,400 and 12,000 particles mm^{-2} were found in the non-seeded and seeded samples, respectively (Tables 1, S1). Although the particles were spread non-homogeneously over the pad, and the numerical estimates can be biased, the seeded sample evidently produced markedly more fine particles than the non-seeded one. Based on the adhesion of the fine particles to the silicon pad (chapter 3.2.4), we suppose the particles were formed by the brine crystallizing at the bottom of the frozen sample, which is in contact with the cooling stage. 3. Larger flakes (tens of micrometres in size) of an irregular shape appeared on the surface of the frozen samples during the sublimation (Figures 7b, 8, and 9). When the ice underneath these flakes sublimed, they detached from the surface but remained slightly fixed to the actual sample. As the frozen sample was retreating due to the sublimation, the flakes kept approaching to the centre of the sample until they fell down onto the stage (Figures 8 and 9). Thus, the flakes were scarcely

https://doi.org/10.5194/tc-2021-376
Preprint. Discussion started: 11 March 2022

found within the periphery, but their abundance increased towards the centre of the sublimated sample. Although we observed the flakes right on the ice surface, the crystallized brine had supposedly originated also from inside the frozen sample, as the sublimating ice continuously exposed deeper layers of the sample (such as the veins previously hidden in the bulk).

Compared to both the non-seeded and the seeded samples, the structures of the sublimation residua from the LN-frozen sample were completely different (Figure 7e, f), forming large fluffy tufts of salt having a lichen-like appearance. The smaller aggregates exhibited a size of about 100 µm, but the large ones exceeded the dimension of our field of view, which is about 400 µm. Unlike the other two freezing methods, the LN technique did not produce any salt rim on the original circumference of the sample, as the sample had already been much below the T_{eu} when transferred onto the cold stage of the ESEM.

3.2.2 Concentration of 0.05 M

The sublimation residua of the 0.05 M samples are displayed in Figure 10. The sublimation yielded structures similar to those described above for the lowest concentration. In the non-seeded and seeded samples, the salt rim remained at the former circumference (Figure 10a, c). The fine salt particles that formed at the bottom of the frozen samples maintained a width of ~1 µm but often were longer than this size (Figures 10a, 10d, 11), and they even interconnected into web-like structures instead of producing separated crystals (Figure 10c). The image analysis with Mountains® software (Digital Surf) detected approximately 39,000 and 60,000 particles mm^{-2} in the non-seeded and the seeded 0.05 M samples, respectively (Tables 1, S1). At this concentration, too, the seeded sample yielded many more fine particles than the non-seeded one. Large tufts of aggregated lichen-like structures, formed probably by the brine crystallizing in the veins between the ice grains, were abundant in the central part of the sublimed samples (Figure 10b, d). Having sizes of tens to hundreds of micrometres, the tufts were much larger than the salt flakes in the 0.005 M samples. The sublimation of the 0.05 M LN-frozen sample yielded even larger lichen-like fluffy tufts, with the dimensions often exceeding 400 µm (Figure 10f). We did not find any small (units or tens of micrometres) crystals in the sublimation residua of the LN-frozen sample.

3.2.3 Concentration of 0.5 M

The structures of these sublimation residua differed significantly from those revealed at lower concentrations. All of the sublimation residua retained the original shapes of the frozen samples, forming ice casts (Figure 12). The surface of the sublimated non-seeded sample was covered with a fibrous film of salt, through which hollows of various sizes were visible (Figure 12a); however, most of the structure underneath the film remained hidden. The situation differed in the sublimated seeded sample (Figure 12b), where almost no film of salt was present on the surface, allowing the inner structure to be clearly discernible. The well-resolved fibrous ice casts formed after the ice had sublimed; these hollows in the salt matrix apparently retained the original sizes and shapes of the sublimed ice crystals. This structure resembled the cells of a honeycomb. In the LN-frozen samples, a sponge-like structure appeared after the sublimation of both the LN-frozen droplet (Figure 12c) and the LN-frozen microspheres (Figure 12d). The pores in the structure were numerous but much smaller than in the samples prepared

https://doi.org/10.5194/tc-2021-376
Preprint. Discussion started: 11 March 2022

via the other freezing methods. The formation of such self-supportive structures indicates that the brine channels in the 0.5 M samples are extensively interconnected.

3.2.4 Adhesion of the salt particles to the silicon pad of the cooling stage

The microscopic images did not allow us to determine if the salt particles were firmly affixed to the cooling stage or lay on the silicon surface freely. Therefore, we tested the adhesivity of the fine particles and larger aggregates to the silicon pad of the cooling stage in the 0.05 M non-seeded sample. After the ice sublimation was completed, we imaged the chosen spot of the sample (which contained both the fine particles and the aggregates, Figure S3a), aerated the ESEM, and opened the specimen chamber. Aerating the chamber alone sufficed for most of the aggregates to fly away. Additionally, we blew upon the sample a gentle stream of air from an air gun to close and evacuate the chamber; subsequently, we imaged the same spot after the aeration/air blowing (Figure S3b). By this process, most of the aggregates were removed, while the fine particles stayed almost intact; thus, the particles had probably been firmly affixed to the stage, but the salt flakes and tufts lay on it without any fixation. These results are in accordance with our inspection of the sublimation process, where the fine particles appeared from below the frozen sample (they had likely formed in its bottom part, in direct contact with the cooling stage), and the flakes and tufts surfaced on the frozen sample and fell on the ground after the ice had sublimated (they had likely formed on the surface and in the body of the ice matrix).

3.2.5 Supercooled brine beyond the edge of a frozen sample below the T_{eu}

During our experiments, we often detected tiny brine droplets beyond the salt rim, where no observable frozen sample had been previously present. These microdroplets did not crystallize at the eutectic temperature and stayed supercooled (Figure 13a), even though the brine in the sample (in the left part of the panel in Figure 13a) had already fully solidified. Evaporation of water from the microdroplets resulted in salt crystallization and formation of a large number of (often) rectangular crystals (Figure 13b). Such supercooled brine microdroplets (and corresponding salt microcrystals) behind the circumference of the original sample were detected routinely in the non-seeded and the seeded samples of all tested concentrations; however, they were absent from the LN-frozen samples below the T_{eu}. A plausible explanation for this behaviour is given in section 4.5.

3.3 Evaporation

The evaporation of the liquid CsCl solution in the ESEM was very quick: The droplet evaporated before we evacuated the specimen chamber and made the ESEM ready for the imaging. The evaporated sample exhibited a wide salt ring at the periphery (Figure 14a, c) and mostly dendritic, sword-like salt crystals in the central part (Figure 14b, d). The evaporation residua resembled to some extent the sublimation ones above the T_{eu}.

https://doi.org/10.5194/tc-2021-376
Preprint. Discussion started: 11 March 2022

4 Discussion

We observed the sublimation, evaporation, and structure of the residua of the CsCl solutions under various conditions (the concentration of the salt, the freezing method, and the sublimation temperature) in the ESEM. Although the project focused on identifying the parameters important for the formation of SSAs, the experiments utilized CsCl salt instead of sea salt of a complex composition. This salt had been chosen for two reasons: 1. A very good contrast between the caesium and the ice in the BSE detector, allowing the liquid brine and solidified salt to be easily distinguished from the ice crystals. Due to this contrast, we were able to monitor the whole process of sublimation, not only the structure of the residua. For example, we were able to assign the original location of various salty structures within frozen samples. 2. The T_{eu} of the CsCl solution (the published values range from −24.83 to −22.3 °C (Chen et al., 2005; Cohen-Adad and Lorimer, 1991; Dubois et al., 1993; Fujiwara and Nishimoto, 1998; Gao et al., 2017; Monnin and Dubois, 1999)) is very close to that of the NaCl (−21 °C (Rodebush, 1918)), by far the most abundant salt present in seawater. Both salts (CsCl and NaCl) can therefore be expected to exhibit a similar tendency to crystallize. However, seawater contains also other salts, which crystallize at various temperatures (e. g. ikaite and mirabilite have much higher eutectic point than NaCl) and may possibly perform certain secondary tasks, including acting as the nucleation centres for the NaCl. Relevant details are nevertheless not covered within this study. However, mirabilite formed at warmer temperatures (−6 to −8 °C) mostly remains in the matrix of the ice, and its crystals embedded in the ice are not easy to be lifted by winds to form aerosol particles. This is evidenced by the sulphate depletion in aerosol, snow and ice samples measured inland Antarctica (Wagenbach et al., 1998; Rankin and Wolff, 2003; Jourdain et al., 2008; Legrand et al., 2017). We would like to mention that we have studied the sublimation of sea salt–ice mixtures lately, and the overall sublimation behaviour was very similar to the one presented in the current study (data not shown). However, CsCl grant much better contrast allowing the observation of subtle features otherwise hardly discernible. Moreover, the sublimation of the frozen samples in the ESEM was carried out at the pressure of 500 Pa, which is much lower than that of atmospheric conditions. Our experimental salt and pressure differ from their natural counterparts, where sea salt-contaminated snow or ice sublime. Despite this discrepancy, important factors affecting the structures of the sublimation residua and their potential to form salt aerosols are revealed in this study (Figure 15, and such factors might be applied also to the formation of natural SSAs.

4.1 Sublimation above the T_{eu}

The sublimation temperature is likely the most important factor determining the preference of the formation of fine salt crystals over a large compact piece of salt. Here, the principle is validated for multiple freezing methods. Should the sublimation take place at a temperature above T_{eu}, the formation of large compact pieces of salt is preferable in all the concentrations and freezing methods tested in this study (Figures 3-5); however, the amount of salt in the central part of the low concentration residua might be low enough to facilitate the formation of small isolated salt particles (Figure 3). The results are consistent with those we obtained previously for the sublimation of the NaCl frost flowers at temperatures of −5 to −17°C (Yang et al.,

https://doi.org/10.5194/tc-2021-376
Preprint. Discussion started: 11 March 2022

2017). The concentration and freezing method seem to affect the resulting structures of the sublimation residua above the T_{eu} only marginally. In most of the experiments, at −20 °C, these compact salt pieces were arranged in a pattern of concentric circles. The probable explanation for this behaviour is as follows: At temperatures above the T_{eu}, the brine is in the liquid state and accumulates immediately beyond the edge of the sample. Apart from ice sublimation, the evaporation of water from the brine proceeds, and the brine that is not in close contact with the ice is prone to crystallization. The tendency of the sample to sublimate or evaporate can be expressed in terms of saturated vapour pressures above the ice and the brine, respectively. At −20 °C, the saturated vapour pressure above ice is 103 Pa (Wexler, 1977). Further, the saturated vapour pressure above the brine can be approximated by Raoult's law (Eq. 1):

$$p = x \cdot p^*, \quad (1)$$

where p is the saturated vapour pressure above the brine, p^* is the saturated vapour pressure of pure water, and x is the mole fraction of water in the brine. At −20 °C, the p^* of supercooled water is 22 Pa higher than the vapour pressure above ice (Murphy and Koop, 2005), equalling 125 Pa. The eutectic molality (at −23 °C) of the CsCl in the brine is 7.7485 mol kg^{-1}; at −20 °C, the equilibrium molality of the CsCl in the brine reaches about 7.2 mol kg^{-1} (Gao et al., 2017). Such a value corresponds to the mole fractions of 0.115 (for the salt) and 0.885 (for water). The estimated vapour pressure above the brine thus attains 111 Pa. The vapour pressure above the brine at −20 °C is then slightly higher than that above the ice, and the evaporation from the brine is expected to be preferred slightly more than the sublimation of ice. Nevertheless, as the difference is small, both processes occur simultaneously. The sublimation of the ice only shrinks the sample, without disturbing the equilibrium, while the evaporation of water from the brine causes its supersaturation. The brine that is in close contact with the ice can compensate for the water lost through ice melting to sustain the equilibrium brine concentration, and thus the brine remains liquid. However, the ice melting cannot supply the water lost by evaporation from the brine at the very edge of the sample. Therefore, only the brine at the edge of the sample, far from the ice, becomes crystalline above the T_{eu}. In due time, the sublimation and evaporation lead to a shrinkage of the sample and the subsequent accumulation of the brine beyond the edge, followed by crystallization of the brine; the processes described above iterated slightly closer to the centre of the sample. As a result, the pieces of crystallized salt are arranged in the observed pattern of concentric (semi)circles (Figures 2-6). These patterns of the sublimation residua (formed above the T_{eu}) resemble those of the "stick-slip" mechanism observed in TiO_2 nanoparticles from evaporating ethanol (Moffat et al., 2009). This process stands in-between the extremes of pined and mobile contact lines evaporation (Deegan et al., 1997; Giorgiutti-Dauphiné and Pauchard, 2018).

The obtained results seem to indicate that the formation of salt aerosols at temperatures above the T_{eu} is improbable due to the crystallization of the liquid brine into large pieces of salt unless the salt concentration is very low. Moreover, the crystalline salt firmly adheres to the silicon pad of the cooling stage and cannot be windblown in our experimental conditions. In nature, however, the base of the saline ice is different, and the sublimating subsurface ice could facilitate aerosolization of the small saline particles. By extension, a large amount of small salt particles and fine structures that might act as a source of salt aerosols can generate only at temperatures below the T_{eu}.

https://doi.org/10.5194/tc-2021-376
Preprint. Discussion started: 11 March 2022


The Cryosphere Discussions

4.2 Sublimation below the T_{eu}: the effect of salt concentration

The structures of the sublimation residua that formed below the T_{eu} strongly depended on the concentration: Low concentrations produced small isolated particles and small aggregates, while high ones resulted in large aggregates and self-supporting structures (Table 2, Figure 15). At low solute concentrations, the amount of the brine is too small to allow the veins in a frozen sample to interconnect sufficiently, and therefore the structures of the veins break apart in the process of the ice sublimation (Figure 7). The sublimation of the samples with low or medium salt concentrations leads to the formation of fine salt particles, small salt flakes, or aggregates, each prevailing in a distinct region of the drop. The well-preserved regular lines of the small salt crystals on the surface of the silicon pad in the non-seeded and seeded droplets at the two lower concentrations enable us to grasp the original lamellar or cellular arrangement of ice and brine. The morphology of ice is closely related to particular freezing temperatures (Schremb and Tropea, 2016; Shibkov et al., 2003). The spacing of the lamellae depends on the freezing rate and solute concentration (Maus, 2007; Rohatgi and Adams, 1967; Wettlaufer, 1992). Based on the appearance of the residua, we deduce that the lowest salt concentration exhibits the highest proportion of fine particles over larger aggregates, and the ratio decreases with increasing concentration. From this perspective, the lowest salinity samples appear to be the best generators of small aerosolizable particles. Conversely, the absolute number of fine salt particles generated per mm2 of the frozen sample substantially increased when the concentration rose from 0.005 to 0.05 M (the estimated number of the salt particles rose 11 and 5 times in non-seeded and seeded samples, respectively; Tables 1, S1) but then abruptly decreased at 0.5 M, as the highly concentrated sample did not yield any smaller salt particles and a self-supporting structure was formed instead. Thus, low to middle salt concentrations are required in order to generate small aerosol-sized particles below the T_{eu}, and samples with the middle salt concentration can be even more effective in producing aerosolable particles than those having the low concentration. As we have not acquired enough reliable data on the relationship between salt concentration and number of small particles, we do not attempt to extrapolate or estimate the number of small particles from samples having lower concentrations than the tested ones. Neither we can estimate the concentration at which the maximum number of small particles is formed.

Although adhesion of the fine particles to the pad was detected in our experiments, the effect might be irrelevant in natural samples. In Arctic conditions, the underlying ice and snow would most probably serve as the basis for the fine particles, and these would be released by the sublimation of such a ground layer. Small flakes and aggregates are not affixed to the stage and can be windblown or split, possibly forming aerosol particles. During the sublimation, the particles are carried by the shrinking sample towards its centre, where they accumulate. A very similar behaviour was described and explained previously in the sublimation of a frozen colloidal suspension (Jambon-Puillet, 2019); the authors of the referenced study proposed that the stains from the freeze-dried drops depend on the initial geometry of the drop, not on the sublimation rate. By extension, the behaviour of the crystallised salt particles below the T_{eu} is approximable by the sublimation of the frozen colloidal suspension, as in neither of the cases are the solidified solutes inside the frozen sample capable of flowing.

https://doi.org/10.5194/tc-2021-376
Preprint. Discussion started: 11 March 2022

High solute concentrations yield a large amount of the brine, which is sufficiently interconnected throughout the sample; such a scenario then leads to the formation of relatively stable and large self-supporting structures (Figure 12). However, these fine structures are expected to exhibit poor mechanical stability against external forces (including, for example, wind-cropping or physical collision with large mobile particles), and their potential breakdown could also lead to the production of small aerosol-sized particles.

4.3 Sublimation below the T_{eu}: the effect of the freezing method

At the two lower concentrations, the structures and sizes of the salt residua were very similar in the non-seeded and seeded samples, while in the sublimated LN-frozen sample the residua formed markedly larger pieces. This effect is supposedly due to the fact that during the LN-freezing the sample freezes from the outside, and the freeze-concentrated brine is expelled by the growing ice towards the interior of the sample. Such sub-surface brine inclusions were revealed in LN-frozen spheres of aqueous solutions already previously (Vetráková et al., 2019). As an excess of the salt forms inside the sample, and the ice crystals emanated during the fast freezing are small, the veins between the ice crystals in the frozen sample may be more interconnected, and thus the resulting sublimation residua form structures larger than those delivered by the other two freezing methods.

At both the 0.005 and 0.05 M concentrations, the surface density of the fine salt particles in the seeded samples largely outnumbered that in the non-seeded samples (Tables 1, S1; 12,000 vs 3,400 mm^{-2} at 0.005 M and 60,000 vs 39,000 mm^{-2} at 0.05 M). Therefore, seeding favours the formation of aerosolable salt particles significantly more than spontaneous freezing.

At the concentration of 0.5 M, the freezing method was a major factor determining the structures of the sublimation residua (Figure 12). Under these conditions, the solidified brine forms self-supporting structures that delineate the shapes of the ice crystals. The structures of these residua therefore depend on the sizes of the ice crystals and the location of the salt in the frozen sample prior to sublimation, i.e. the result of the sublimation is the salty cast. The variation of the outcomes of the three freezing methods (Figure 12) is striking: The surface of the non-seeded sample is covered with a layer of crystalline salt (Figure 12a). This effect corresponds to the results of our previous studies (Vetráková et al., 2019, 2020) in terms of the accumulation of the solutes on the surface of the non-seeded sample, as in a globally supercooled sample cooled from the bottom the freezing proceeds from the bottom upwards (Figure 1A). The observed surface "skin" restricts to a large extent the access to the interior of the sample, thus preventing the more subtle and possibly fragile parts from being easily withdrawn by the blowing winds. Conversely, the seeding promoted freezing downwards from the surface, where the nucleating crystal had been placed (Figure 1B). For this reason, no accumulation of the brine on the surface of the seeded sample is either expected or observed, allowing the internal structure to be nicely visible. Under this concentration (0.5 M) and freezing method, the formed ice crystals were very oblong, with strong parallel arrangement (Figure 12b). The resulting ice casts remained well preserved after the ice sublimation, enabling us to observe that not only the veins (triple junctions, i.e. places where three ice crystals meet) but also the whole grain walls were filled with an amount of brine sufficient to support the structure. In the LN-frozen sample, the pores in the sublimation residua were much smaller, as abrupt freezing in LN induces the formation of small ice crystals. A

https://doi.org/10.5194/tc-2021-376
Preprint. Discussion started: 11 March 2022

comparison of the images in Figure 12c and 12d will reveal that the size of the sample does not determine the sizes of the ice crystals: The submillimetre spheres and millimetre-sized droplet exhibit similar dimensions of the pores in the residual structures. The structures hold together in large pieces even after the ice sublimation, with no collapse observed. By inspecting the sponge-like features in the detailed image of the LN-frozen residua provided in the bottom-left corner of Figure 12c, we established that the structure of the residua delineates the veins between the ice crystals, not the whole grain boundaries, as in the seeded sample. Moreover, the internal structures of the sublimated LN-frozen samples appear denser than those of the seeded sample, due to the very different freezing rates and directionalities: Freezing from the outside expels the brine towards the interior of the sample, as demonstrated in Figure 1C.

4.4 Evaporation above 0 °C

We took a step further and observed the evaporation of the aqueous solution at +2 °C. Such conditions resemble the behaviour of sea water at solid supports on coastlines and grounds after the melting of sea ice (Keene et al., 2007). As the diameter of the observed drops is about 4 mm, they are much larger than the jet-burster bubbles, which embody the most common sources of the sea aerosols. The evaporation residua resembled to some extent those formed by the sublimation above the T_{eu}. This is not surprising, because the evaporation-crystallization mechanisms of both the processes are similar (the salt in the frozen sample above T_{eu} is dissolved in the liquid brine and evaporation of water from the brine induces salt crystallization).

4.5 Precursor nanofilm formed below 0 °C

What is the origin of the supercooled microdroplets found beyond the perimeter of original frozen samples? We presume a small portion of a sample solution spread over the silicon pad and formed a thin film (invisible for the ESEM) due to surface wetting during the freezing while the temperature was still above the T_{eu}. Due to the evaporation, micrometric droplets were produced from the film; enhanced salt concentration in the microdroplets enabled their visualization in the ESEM. Further evaporation led to salt crystalization. The generation of small crystals behind the perimeter of the visible sample was noticed in all samples whose temperature exceeded the T_{eu} during the experiments (Figures 4, 5, 13) - they were routinely present in the non-seeded and seeded samples, but absent in the LN-frozen samples below the T_{eu}. What, then, is a plausible explanation for this difference? The non-seeded and the seeded samples had been loaded on the cooling stage in the liquid state and subsequently frozen, while the LN-frozen samples were treated externally and had already fully solidified before being loaded on the stage. Therefore, we assume that the observed effect relates to the interaction of a solution with the silicon surface. Previously, wetting the upper molecular layers of a silicon (1,0,0) surface with water was simulated (Barisik and Beskok, 2013; Ozcelik et al., 2020); the researchers observed the water spread beyond the drop boundary. The nanometre-sized crystals observed centimetres away from the creeping front were considered a proof of precursor nanofilms (Qazi et al., 2019). Our findings not only confirm such nanofilms in CsCl solutions but also reveal their formation around salty ices at temperatures above the salts' eutectics. The salt leakage through precursor nanofilms at sub-zero centigrade temperatures can embody a viable mechanism of spreading the salts to the previously pristine snow in arctic conditions.

https://doi.org/10.5194/tc-2021-376
Preprint. Discussion started: 11 March 2022

4.6 Implications to polar atmosphere and environment

This study identifies the conditions at which the sublimation of salty frozen samples generates small particles of salt that may potentially become a source of salt aerosols. 0.005, 0.05, and 0.5 M CsCl equal to 0.84, 8.3, and 78‰ (psu), respectively. With this concentration values we wanted to mimic the broad range of salinities in the environment, from low salinity surface snows in Arctic coastal regions to high salinity sea ice (formed from approx. 0.5 M seawater). We showed that the formation of the small particles is restricted if the brine is liquid during the ice sublimation, i.e., at temperatures higher than the T_{eu}. The sublimation temperature appears to be the most critical parameter in this respect. In the given context, we can comprehend the fact that previous studies did not succeed in seeking the SSA production from the frost flowers in a wind tunnel (Roscoe et al., 2011) and in an ESEM (Yang et al., 2017). In the former article, although the cold chamber air temperatures in most of the experiments were −30 °C or lower, the measured ice temperature reached −5 °C (Howard Roscoe and Eric Wolff, personal communications), and the temperature of the sampling line was about −10 °C (Roscoe et al., 2011). In the latter one, the sublimation of the brine-covered frost flowers at the temperatures of −5 and −17 °C yielded a large chunk of salt (Yang et al., 2017). In both of the studies, the temperature of the frost flowers was well above the T_{eu}; in that respect, the lack of aerosol-forming particles is in good agreement with the results of our study.

The argument for the frost flowers being a source of the SSA was threefold: (1) whether they are sulphate-depleted; (2) whether they break and form small particles; and, finally, (3) whether they cover enough area to be relevant. When the ice temperature ranges below −6.4°C, which is a typical situation in a polar winter and spring, mirabilite ($Na_2SO_4 \cdot 10\ H_2O$) precipitates out from the brine, and therefore the frost flowers growing from the brine are sulphate-depleted, as seen in the observations (e.g. Rankin and Wolff, 2003). The temperature gradients above the thin ice are strong, but it is unlikely that the temperature of newly grown frost flowers is below the T_{eu}, except for the tips of the flowers. However, when sea ice becomes thicker, ice surface temperature will approach that of the air and may decrease below the T_{eu}, making aged frost flowers more prone to generating SSAs, on condition that the brine concentration is low enough. Nevertheless, the aged frost flowers are more likely to have been buried by precipitation of snowfall, reducing the opportunity for the frost flowers to serve as a source of SSA.

Both the recent field data (Frey et al., 2020) and the modelling (e.g., Huang and Jaeglé, 2017; Levine et al., 2014; Rhodes et al., 2017; Yang et al., 2019) have demonstrated the importance of airborne saline snow particles as a source of the SSA in polar regions. The salty snow lying on the sea ice has also the potential to generate the SSA at temperatures below the T_{eu}. On average, the snow salinity is several orders of magnitude lower than that of sea water and frost flowers (Frey et al., 2020). Thus, according to the results presented herein, the snowpack is supposed to yield smaller salt particles and fine structures of salts upon sublimation at very low temperatures, and, therefore, to be potentially an effective source of the SSA. However, there might be significant differences depending on whether the snowpack lies on young sea ice or multi-year sea ice, and whether there is flooding, which depends on snow thickness vs. ice thickness. Normally, young sea ice is thin and thus relatively warmer than thick ice, and a temperature as low as the T_{eu} could be difficult to reach on very thin young ice. Therefore, the snowpack on multi-year ice is more likely to form fine salt structures and SSA than the snow on relatively thin

https://doi.org/10.5194/tc-2021-376
Preprint. Discussion started: 11 March 2022

sea ice. There are many other factors that may affect the structure of the residua – e. g. salt crystallographic system, activity of the brine solution, or geometry of the cooling environment. Finally, we should also note that the formation of the sublimation residua will probably be accompanied by acidity changes during both the freezing and the sublimation (Vetráková et al., 2017) which may have major consequences as regards the heterogeneous reactivity of the aerosols thus formed (Pratt et al., 2013).

The implications of our findings to the polar atmosphere and environment are significant; however, further data (field, laboratory and modelling) are still necessary to confirm the conclusions.

4.7 Connection to the morphology and properties of the original frozen samples

The observed morphologies of the sublimation residua formed below the T_{eu} bear important information about the internal environment of the original frozen samples. We previously studied the properties of the frozen samples from which the residua had formed (Vetráková et al., 2019). In the relevant article, the differences in the surface morphologies were well visible, but the observation of the interiors was insufficient. The brine structures visible on the ice surfaces and the sublimation residua of the spontaneously frozen samples sublimed at -25 °C are compared in Figure 16.

The sublimation below the T_{eu} in the research reported herein allowed us to inspect also the sub-surface morphology by the ESEM more thoroughly. Another method for the direct visualization of solute locations was µCT (Hullar and Anastasio, 2016). The technique provided a 3D scan of the location of impurities in ice, but the resolution was much coarser than that achieved with the ESEM (~16 and 2 µm in the µCT vs ~500 and 50 nm in the ESEM for an overview and details, respectively). Thus, the researchers were able to visualize larger inclusions of brine in the ice, but the brine in the veins (65 to 88 wt% of the salt) was beyond the detection ability of the µCT method. The deduction of the morphology of a frozen sample from the morphology of a sublimation residuum can now supply the missing piece of the puzzle.

There appear to be several characteristic domains where impurities can accumulate within ice – on the surface, at the grain boundaries, in liquid inclusions, or within the ice crystals (Bartels-Rausch et al., 2014; Blackford et al., 2007; Dominé et al., 2003; Hullar and Anastasio, 2016; Light et al., 2009). The existence of various microenvironments in the vicinity of guest molecules within ice was also observed spectroscopically (Heger et al., 2011; Heger and Klán, 2007; Krausko et al., 2014; Ondrušková et al., 2018). The location of impurities in ice and snow is an important factor for their reactivity and potential release to the atmosphere, due to considerable variations in the accessibility of gas-phase oxidants and photons in the domains (Hullar and Anastasio, 2016 and the references within). For example, our experimental results indicate that the LN-frozen microspheres contain most of the brine inside the ice, not on the surface (Vetráková et al., 2020). It remains an open question if the molecules on the surface of the frozen microsphere are exposed to the incoming radiation or reactive gasses to a larger extent than the molecules inside and if and how the accessibility of these compartments depend on the temperature (Ray et al., 2011).

https://doi.org/10.5194/tc-2021-376
Preprint. Discussion started: 11 March 2022

When comparing the sublimation residua formed below the T_{eu} from the 0.5 M frozen samples (Figure 12), it is obvious that an abundance of the salt on the surface markedly depends on the freezing method. While the non-seeded sample is completely covered with salt, there is no excessive surface salt in the seeded sample and LN-frozen samples. This corroborates our previous observations of the frozen (unsublimated) samples (Vetráková et al., 2019), where the amount of salt on the ice surface was related to the directionality of freezing. Higher amounts of surface salt in the frozen non-seeded sample can thus lead to enhanced oxidation of halogens by atmospheric gases and their release to the atmosphere. The sublimation of ice from the concentrated frozen samples leads to the formation of large salt chunks (above T_{eu}, Figure 5) or highly porous structures (below the T_{eu}, Figure 12). Therefore, the sublimation temperature can significantly affect the accessibility of gases and photons to the salt and thus alter the reactivity within these compartments.

The inspection of the residua formed by the sublimation of the 0.5 M frozen samples below the T_{eu} (Figure 12) indicated substantial differences in the thickness of the brine compartments in the interior of the seeded and the LN-frozen samples. Regrettably, we could not evaluate this parameter in the non-seeded sample, as its surface was covered with a salt film to a large extent and the internal morphology was hidden. In the seeded sample, the salt crystallized in the form of relatively thick walls surrounding individual ice crystals. In the LN-frozen sample, the salt crystallized as very thin tortuous veins – the overall shape of the residuum resembled a sponge. The most important differences between these two preparation methods consisted in the directionality and freezing rate. Seeding is a method of slow freezing from the upper surface (Figure 12b), generating large ice crystals, while LN-freezing proceeds under fast freezing from all sides (Figure 12c), generating small ice crystals (Vetráková et al., 2019). Thus, the freezing rate and/or directionality affect the thickness of the brine compartments in a frozen sample. It is intuitively obvious that the brine surrounding small ice crystals with large specific surface areas needs to spread more, and therefore the grain boundaries and veins containing the salt ought to be thinner than in the sample of identical concentration containing larger ice crystals. In this study, this relationship is proved experimentally (Figure 12b vs. 12c). Previously, slow cooling rates were related to a larger extent of aggregation of impurities in ice, (Heger et al., 2005) while fast cooling rates led to partial vitrification of the brine (Imrichová et al., 2019; Ondrušková et al., 2020), presumably due to confined space and more efficient cooling of thin veins. The subtle differences in the ice-impurity morphology can possibly alter the immediate molecular environment and consequently variate the absorption (Bononi et al., 2020), aggregation (Kania et al., 2014), pH changes, (Heger et al., 2006) and, therefore, also the reactivity of compounds and their photochemical quantum yields (Hullar et al., 2018; Kahan and Donaldson, 2007; Klánová et al., 2003). An important effect associated with the freezing of salts (and buffer solutions in particular (Gomez et al., 2001; Sundaramurthi et al., 2010; Vetráková et al., 2017)) is the freezing-induced pH shift (e.g. Bronshteyn and Chernov, 1991; Heger et al., 2006a; Workman and Reynolds, 1950). The pH shift greatly affects the stability and reactivity of compounds in a frozen sample (Krausková et al., 2016; Takenaka et al., 2006). However, the freezing-induced pH-shift was found mostly diminished after ice sublimation (Vetráková et al., 2017) in the particular case of phosphate buffers, and the acidity changes that the compounds underwent during the freezing step on their path from a solution to a sublimation residue cannot be directly evaluated without knowledge of the history of the sample.

https://doi.org/10.5194/tc-2021-376
Preprint. Discussion started: 11 March 2022

Herein we observed several characteristic units among the sublimation residua. The residua formed above the T_{eu} cannot be assigned to particular domains in the ice, because liquid brine from the individual domains pours together after the ice has sublimated. However, the flow of the crystallized salt below the T_{eu} is restricted, and the shape of the residua (fine particles, salt flakes, and lichen and sponge-shaped tufts) partially mirrors the one of the domains in the ice. From our observations of the sublimation processes, we deduce the genesis of the individual salt features as follows: Fine salt particles are likely formed by crystallization of the brine in the veins at the bottom of the sample. Arguments supporting this opinion were already outlined above (adhesion of the particles to the cooling pad, their visual absence on the gradually sublimated ice surface). However, we cannot exclude that a portion of the fine particles comes from thin or separated veins inside the ice body that broke to small pieces after ice had sublimated. Remnants of the crystalline salt from larger and more interconnected veins can be presumably found in the form of lichen-like tufts. Lastly, crystallization of the brine in pools on the surface and liquid inclusions in the ice body likely led to formation of 2-dimensional salty flakes. The knowledge of the morphologies brought up in this paper and their relationship to the properties of original frozen samples should be borne in mind when designing laboratory experiments to simulate natural ice and snow. As the properties of frozen samples largely depend on the sample preparation method, artificial samples must be prepared with care in order to mimic natural ice and snow.

5 Summary

In this study we focused on identifying the most suitable conditions for formation of salt aerosols. We observed the sublimation of frozen salty solutions and inspected the morphology and number of the resulting salt particles based on the salt concentration, freezing method and sublimation temperature. CsCl was used as a proxy for natural sea salts due to its excellent visibility within the ice by the ESEM.

We demonstrated that the sublimation temperature is the most important factor for the formation of aerosolable particles upon sublimation of various frozen salty ices. When the sublimation takes place at temperatures above the T_{eu}, the formation of large compact pieces of salt with very little aerosol-forming potential is preferred for all the concentrations and freezing methods tested herein; the concentration and the freezing method seem to play a less important role in the structure of the sublimation residua. Similar effect was observed when a liquid salty solution evaporated. Conversely, the structures of the residua formed at temperatures below the T_{eu} strongly depend on the concentration: Low salinity samples yield small isolated particles and small aggregates that are directly available to be windblown and become salt aerosols; high salinity samples transform into large aggregates with fine structures. Regarding the abundance of the fine particles in various residua, the 0.05 M seeded sample yielded the largest number of fine salt particles and thus would be the most promising source of salt aerosols. The outcomes of this article clearly indicate that the sublimation process on highly saline ices, such as frost flowers lying on young sea ice, does not directly induce the formation of SSAs unless the interconnected salt structures are potentially brought down by external forces, such as physical collision with large mobile particles. On the other hand, less saline snow lying on aged ice is more likely to directly generate separated fine salt particles during the sublimation process at temperatures below the T_{eu}.

https://doi.org/10.5194/tc-2021-376
Preprint. Discussion started: 11 March 2022

Our data emphasize the requirement of very low temperatures for the formation of SSAs. This condition favours salty snow over frost flowers as an efficient source of the SSA, provided that no flooding has occurred.

We are aware of the limitations in using artificial samples to mimic natural processes. However, such systematic study where we vary parameters (sublimation temperature, concentration, freezing method) and monitor the outcome are very difficult (and nearly impossible) to perform with natural samples, as there are many collateral effects in nature that we are not able to fully distinguish and interpret. Nevertheless, evaluation of these effects step by step in a laboratory may be very helpful when interpreting the behaviour of complex natural samples.

Author contributions

Ľ.V. conducted the experiments, analyzed the data, and prepared the manuscript; J.R. operated the ESEM; D.H. and X.Y. developed the idea of the project; and V.N., D.H., and X.Y. contributed to the discussions and writing of the final paper.

Declaration of Competing Interest

The authors declare that they have no known competing financial interests or personal relationships that could have appeared to influence the work reported in this paper.

Acknowledgement

This work was supported by Czech Science Foundation via projects 19-08239S and 19-03909S. We thank Kamila Závacká for performing the DSC experiments and Přemysl Dohnal for the language corrections.

Financial support

This research has been supported by the Czech Science Foundation (grants no. 19-08239S and 19-03909S).

References

Abbatt, J. P. D., Thomas, J. L., Abrahamsson, K., Boxe, C., Granfors, A., Jones, A. E., King, M. D., Saiz-Lopez, A., Shepson, P. B., Sodeau, J., Toohey, D. W., Toubin, C., Von Glasow, R., Wren, S. N. and Yang, X.: Halogen activation via interactions with environmental ice and snow in the polar lower troposphere and other regions, Atmos. Chem. Phys., 12(14), 6237–6271, doi:10.5194/acp-12-6237-2012, 2012.

Barisik, M. and Beskok, A.: Wetting characterisation of silicon (1,0,0) surface, Mol. Simul., 39(9), 700–709, doi:10.1080/08927022.2012.758854, 2013.

https://doi.org/10.5194/tc-2021-376
Preprint. Discussion started: 11 March 2022

Barrie, L. A., Bottenheim, J. W., Schnell, R. C., Crutzen, P. J. and Rasmussen, R. A.: Ozone destruction and photochemical reactions at polar sunrise in the lower Arctic atmosphere, Nature, 334(6178), 138–141, doi:10.1038/334138a0, 1988.

Bartels-Rausch, T., Jacobi, H. W., Kahan, T. F., Thomas, J. L., Thomson, E. S., Abbatt, J. P. D., Ammann, M., Blackford, J. R., Bluhm, H., Boxe, C., Domine, F., Frey, M. M., Gladich, I., Guzmán, M. I., Heger, D., Huthwelker, T., Klán, P., Kuhs, W. F., Kuo, M. H., Maus, S., Moussa, S. G., McNeill, V. F., Newberg, J. T., Pettersson, J. B. C., Roeselová, M. and Sodeau, J. R.: A review of air–ice chemical and physical interactions (AICI): liquids, quasi-liquids, and solids in snow, Atmos. Chem. Phys., 14(3), 1587–1633, doi:10.5194/acp-14-1587-2014, 2014.

Blackford, J. R., Jeffree, C. E., Noake, D. F. J. and Marmo, B. A.: Microstructural evolution in sintered ice particles containing NaCl observed by low-temperature scanning electron microscope, Proc. Inst. Mech. Eng. Part L-Journal Mater. Appl., 221(L3), 151–156, doi:10.1243/14644207jmda134, 2007.

Bononi, F. C., Chen, Z., Rocca, D., Andreussi, O., Hullar, T., Anastasio, C. and Donadio, D.: Bathochromic Shift in the UV-Visible Absorption Spectra of Phenols at Ice Surfaces: Insights from First-Principles Calculations, J Phys Chem A, doi:10.1021/acs.jpca.0c07038, 2020.

Bottenheim, J. W., Fuentes, J. D., Tarasick, D. W. and Anlauf, K. G.: Ozone in the Arctic lower troposphere during winter and spring 2000 (ALERT2000), Atmos. Environ., 36(15–16), 2535–2544, doi:10.1016/S1352-2310(02)00121-8, 2002.

Bronshteyn, V. L. and Chernov, A. A.: Freezing potentials arising on solidification of dilute aqueous-solutions of electrolytes, J. Cryst. Growth, 112(1), 129–145, 1991.

Butler, B. M., Papadimitriou, S. and Kennedy, H.: The effect of mirabilite precipitation on the absolute and practical salinities of sea ice brines, Mar. Chem., 184, 21–31, doi:10.1016/j.marchem.2016.06.003, 2016.

Chen, N. J., Morikawa, J., Kishi, A. and Hashimoto, T.: Thermal diffusivity of eutectic of alkali chloride and ice in the freezing–thawing process by temperature wave analysis, Thermochim. Acta, 429(1), 73–79, doi:10.1016/J.TCA.2004.11.010, 2005.

Cohen-Adad, R. and Lorimer, J. W.: Alkali metal and ammonium chlorides in water and heavy water (binary systems), Pergamon Press. [online] Available from: https://www.sciencedirect.com/science/book/9780080239187 (Accessed 10 April 2018), 1991.

Deegan, R. D., Bakajin, O., Dupont, T. F., Huber, G., Nagel, S. R. and Witten, T. A.: Capillary flow as the cause of ring stains from dried liquid drops, Nature, 389(6653), 827–829, doi:10.1038/39827, 1997.

DeMott, P. J., Hill, T. C. J., McCluskey, C. S., Prather, K. A., Collins, D. B., Sullivan, R. C., Ruppel, M. J., Mason, R. H., Irish, V. E., Lee, T., Hwang, C. Y., Rhee, T. S., Snider, J. R., McMeeking, G. R., Dhaniyala, S., Lewis, E. R., Wentzell, J. J. B., Abbatt, J., Lee, C., Sultana, C. M., Ault, A. P., Axson, J. L., Diaz Martinez, M., Venero, I., Santos-Figueroa, G., Stokes, M. D., Deane, G. B., Mayol-Bracero, O. L., Grassian, V. H., Bertram, T. H., Bertram, A. K., Moffett, B. F. and Franc, G. D.: Sea spray aerosol as a unique source of ice nucleating particles, Proc. Natl. Acad. Sci., 113(21), 5797–5803, doi:10.1073/pnas.1514034112, 2016.

Dominé, F., Lauzier, T., Cabanes, A., Legagneux, L., Kuhs, W. F., Techmer, K. and Heinrichs, T.: Snow metamorphism as

https://doi.org/10.5194/tc-2021-376
Preprint. Discussion started: 11 March 2022

revealed by scanning electron microscopy, Microsc. Res. Tech., 62(1), 33–48, doi:10.1002/jemt.10384, 2003.

Dubois, M., Royer, J. J., Weisbrod, A. and Shutka, A.: Reconstruction of low-temperature binary phase diagrams using a constrained least squares method: Application to the H2O-CsCl system, Eur. J. Mineral., 5(6), 1145–1152 [online] Available from: http://cat.inist.fr/?aModele=afficheN&cpsidt=4022663, 1993.

Frey, M. M., Norris, S. J., Brooks, I. M., Anderson, P. S., Nishimura, K., Yang, X., Jones, A. E., Nerentorp Mastromonaco, M. G., Jones, D. H. and Wolff, E. W.: First direct observation of sea salt aerosol production from blowing snow above sea ice, Atmos. Chem. Phys., 20(4), 2549–2578, doi:10.5194/acp-20-2549-2020, 2020.

Fujiwara, S. and Nishimoto, Y.: Nonbiological Complete Differentiation of the Enantiomeric Isomers of Amino Acids and Sugars by the Complexes of Gases with the Eutectic Compounds of Alkali Chlorides and Water, Anal. Sci., 14(3), 507–514, doi:10.2116/analsci.14.507, 1998.

Gao, D., Li, D. and Li, W.: Solubility of RbCl and CsCl in pure water at subzero temperatures, heat capacity of RbCl(aq) and CsCl(aq) at T = 298.15 K, and thermodynamic modeling of RbCl + H 2 O and CsCl + H 2 O systems, J. Chem. Thermodyn., 104, 201–211, doi:10.1016/j.jct.2016.09.031, 2017.

De Gennes, P. G.: Wetting: statics and dynamics, Rev. Mod. Phys., 57(3), 827, doi:10.1103/RevModPhys.57.827, 1985.

Giorgiutti-Dauphiné, F. and Pauchard, L.: Drying drops: Drying drops containing solutes: From hydrodynamical to mechanical instabilities, Eur. Phys. J. E, 41(3), doi:10.1140/epje/i2018-11639-2, 2018.

Gomez, G., Pikal, M. J. and Rodriguez-Hornedo, N.: Effect of initial buffer composition on pH changes during far-from-equilibrium freezing of sodium phosphate buffer solutions, Pharm. Res., 18(1), 90–97, doi:10.1023/a:1011082911917, 2001.

Heger, D. and Klán, P.: Interactions of organic molecules at grain boundaries in ice: A solvatochromic analysis, J. Photochem. Photobiol. A Chem., 187(2–3), doi:10.1016/j.jphotochem.2006.10.012, 2007.

Heger, D., Jirkovský, J. and Klán, P.: Aggregation of Methylene Blue in Frozen Aqueous Solutions Studied by Absorption Spectroscopy, J. Phys. Chem. A, 109(30), 6702–6709, doi:10.1021/jp050439j, 2005.

Heger, D., Klanova, J. and Klan, P.: Enhanced protonation of cresol red in acidic aqueous solutions caused by freezing, J. Phys. Chem. B, 110(3), 1277–1287, doi:10.1021/jp0553683, 2006.

Heger, D., Nachtigallová, D., Surman, F., Krausko, J., Magyarová, B., Brumovský, M., Rubeš, M., Gladich, I. and Klán, P.: Self-organization of 1-methylnaphthalene on the surface of artificial snow grains: A combined experimental-computational approach, J. Phys. Chem. A, 115(41), doi:10.1021/jp205627a, 2011.

Huang, J. and Jaeglé, L.: Wintertime enhancements of sea salt aerosol in polar regions consistent with a sea ice source from blowing snow, Atmos. Chem. Phys., 17(5), 3699–3712, doi:10.5194/acp-17-3699-2017, 2017.

Hullar, T. and Anastasio, C.: Direct visualization of solute locations in laboratory ice samples, Cryosphere, 10(5), 2057–2068, doi:10.5194/tc-10-2057-2016, 2016.

Hullar, T., Magadia, D. and Anastasio, C.: Photodegradation Rate Constants for Anthracene and Pyrene Are Similar in/on Ice and in Aqueous Solution, Environ. Sci. Technol., doi:10.1021/acs.est.8b02350, 2018.

Imrichová, K., Veselý, L., Gasser, T. M., Loerting, T., Neděla, V. and Heger, D.: Vitrification and increase of basicity in

between ice I h crystals in rapidly frozen dilute NaCl aqueous solutions, J. Chem. Phys., 151(1), 014503, doi:10.1063/1.5100852, 2019.

Jambon-Puillet, E.: Stains from Freeze-Dried Drops, Langmuir, doi:10.1021/acs.langmuir.9b00084, 2019.

Jourdain, B., Preunkert, S., Cerri, O., Castebrunet, H., Udisti, R. and Legrand, M.: Year-round record of size-segregated aerosol composition in central Antarctica (Concordia station): Implications for the degree of fractionation of sea-salt particles, J. Geophys. Res., 113(D14), D14308, doi:10.1029/2007JD009584, 2008.

Kahan, T. F. and Donaldson, D. J.: Photolysis of Polycyclic Aromatic Hydrocarbons on Water and Ice Surfaces, J. Phys. Chem. A, 111(7), 1277–1285, doi:10.1021/jp066660t, 2007.

Kaleschke, L., Richter, A., Burrows, J., Afe, O., Heygster, G., Notholt, J., Rankin, A. M., Roscoe, H. K., Hollwedel, J., Wagner, T. and Jacobi, H. W.: Frost flowers on sea ice as a source of sea salt and their influence on tropospheric halogen chemistry, Geophys. Res. Lett., 31(16), L16114, doi:10.1029/2004GL020655, 2004.

Kania, R., Malongwe, J. K., Nachtigallová, D., Krausko, J., Gladich, I., Roeselová, M., Heger, D. and Klán, P.: Spectroscopic properties of benzene at the air-ice interface: A combined experimental-computational approach, J. Phys. Chem. A, 118(35), doi:10.1021/jp501094n, 2014.

Keene, W. C., Maring, H., Maben, J. R., Kieber, D. J., Pszenny, A. A. P. P., Dahl, E. E., Izaguirre, M. A., Davis, A. J., Long, M. S., Zhou, X., Smoydzin, L. and Sander, R.: Chemical and physical characteristics of nascent aerosols produced by bursting bubbles at a model air-sea interface, J. Geophys. Res., 112(D21), D21202, doi:10.1029/2007JD008464, 2007.

Klánová, J., Klán, P., Heger, D. and Holoubek, I.: Comparison of the effects of UV, H<inf>2</inf>O<inf>2</inf>/UV and γ-irradiation processes on frozen and liquid water solutions of monochlorophenols, Photochem. Photobiol. Sci., 2(10), doi:10.1039/b303483F, 2003.

Krausko, J., Runštuk, J., Neděla, V., Klán, P. and Heger, D.: Observation of a brine layer on an ice surface with an environmental scanning electron microscope at higher pressures and temperatures, Langmuir, 30(19), 5441–5447, doi:10.1021/la500334e, 2014.

Krausková, Ľ., Procházková, J., Klašková, M., Filipová, L., Chaloupková, R., Malý, S., Damborský, J. and Heger, D.: Suppression of protein inactivation during freezing by minimizing pH changes using ionic cryoprotectants, Int. J. Pharm., 509(1–2), 41–49, doi:10.1016/j.ijpharm.2016.05.031, 2016.

Legrand, M., Preunkert, S., Wolff, E., Weller, R., Jourdain, B. and Wagenbach, D.: Year-round records of bulk and size-segregated aerosol composition in central Antarctica (Concordia site) – Part 1: Fractionation of sea-salt particles, Atmos. Chem. Phys., 17(22), 14039–14054, doi:10.5194/acp-17-14039-2017, 2017.

Levine, J. G., Yang, X., Jones, A. E. and Wolff, E. W.: Sea salt as an ice core proxy for past sea ice extent: A process-based model study, J. Geophys. Res. Atmos., 119(9), 5737–5756, doi:10.1002/2013JD020925, 2014.

Light, B., Brandt, R. E. and Warren, S. G.: Hydrohalite in cold sea ice: laboratory observations of single crystals, surface accumulations, and migration rates under a temperature gradient, with application to “snowball earth,” J. Geophys. Res. Ocean., 114(7), 1–17, doi:10.1029/2008JC005211, 2009.

Maus, S.: Prediction of the cellular microstructure of sea ice by morphological stability theory, in Physics and Chemistry of Ice, edited by W. F. Kuhs, pp. 371–382, RSC Publishing., 2007.

Michaloudi, E., Papakostas, S., Stamou, G., Neděla, V., Tihlaříková, E., Zhang, W. and Declerck, S. A. J.: Reverse taxonomy applied to the brachionus calyciflorus cryptic species complex: Morphometric analysis confirms species delimitations revealed by molecular phylogenetic analysis and allows the (re) description of four species, PLoS One, doi:10.1371/journal.pone.0203168, 2018.

Moffat, J. R., Sefiane, K. and Shanahan, M. E. R.: Effect of TiO2 Nanoparticles on Contact Line Stick−Slip Behavior of Volatile Drops, J. Phys. Chem. B, 113(26), 8860–8866, doi:10.1021/jp902062z, 2009.

Monnin, C. and Dubois, M.: Thermodynamics of the CsCl-H2O system at low temperatures, Eur. J. Mineral., 11(3), 477–482, doi:10.1127/ejm/11/3/0477, 1999.

Murphy, D. M. and Koop, T.: Review of the vapour pressures of ice and supercooled water for atmospheric applications, Q. J. R. Meteorol. Soc., 131(608), 1539–1565, doi:10.1256/qj.04.94, 2005.

Neděla, V.: Methods for additive hydration allowing observation of fully hydrated state of wet samples in environmental SEM, Microsc. Res. Tech., 70(2), 95–100, doi:10.1002/jemt.20390, 2007.

Neděla, V., Tihlaříková, E., Runštuk, J. and Hudec, J.: High-efficiency detector of secondary and backscattered electrons for low-dose imaging in the ESEM, Ultramicroscopy, 184, 1–11, doi:10.1016/j.ultramic.2017.08.003, 2018.

Neděla, V., Tihlaříková, E., Maxa, J., Imrichová, K., Bučko, M. and Gemeiner, P.: Simulation-based optimisation of thermodynamic conditions in the ESEM for dynamical in-situ study of spherical polyelectrolyte complex particles in their native state, Ultramicroscopy, 211, 112954, doi:10.1016/j.ultramic.2020.112954, 2020.

O'Dowd, C. D., Lowe, J. A., Smith, M. H. and Kaye, A. D.: The relative importance of non-sea-salt sulphate and sea-salt aerosol to the marine cloud condensation nuclei population: An improved multi-component aerosol-cloud droplet parametrization, Q. J. R. Meteorol. Soc., 125(556), 1295–1313, doi:10.1002/qj.1999.49712555610, 1999.

Ondrušková, G., Krausko, J., Stern, J. N., Hauptmann, A., Loerting, T. and Heger, D.: Distinct Speciation of Naphthalene Vapor Deposited on Ice Surfaces at 253 or 77 K: Formation of Submicrometer-Sized Crystals or an Amorphous Layer, J. Phys. Chem. C, 122(22), doi:10.1021/acs.jpcc.8b03972, 2018.

Ondrušková, G., Veselý, L., Zezula, J., Bachler, J., Loerting, T. and Heger, D.: Using Excimeric Fluorescence to Study How the Cooling Rate Determines the Behavior of Naphthalenes in Freeze-Concentrated Solutions: Vitrification and Crystallization, J. Phys. Chem. B, 124(46), 10556–10566, doi:10.1021/acs.jpcb.0c07817, 2020.

Ozcelik, H. G., Ozdemir, A. C., Kim, B. and Barisik, M.: Wetting of single crystalline and amorphous silicon surfaces: effective range of intermolecular forces for wetting, Mol. Simul., 46(3), 224–234, doi:10.1080/08927022.2019.1690145, 2020.

Peterson, P. K., Pöhler, D., Sihler, H., Zielcke, J., General, S., Frieß, U., Platt, U., Simpson, W. R., Nghiem, S. V., Shepson, P. B., Stirm, B. H., Dhaniyala, S., Wagner, T., Caulton, D. R., Fuentes, J. D. and Pratt, K. A.: Observations of bromine monoxide transport in the Arctic sustained on aerosol particles, Atmos. Chem. Phys., doi:10.5194/acp-17-7567-2017, 2017.

Pratt, K. A., Custard, K. D., Shepson, P. B., Douglas, T. A., Pöhler, D., General, S., Zielcke, J., Simpson, W. R., Platt, U.,

Tanner, D. J., Gregory Huey, L., Carlsen, M. and Stirm, B. H.: Photochemical production of molecular bromine in Arctic surface snowpacks, Nat. Geosci., 6(5), 351–356, doi:10.1038/ngeo1779, 2013.

Qazi, M. J., Salim, H., Doorman, C. A. W., Jambon-Puillet, E. and Shahidzadeh, N.: Salt creeping as a self-amplifying crystallization process, Sci. Adv., 5(12), doi:10.1126/SCIADV.AAX1853/SUPPL_FILE/AAX1853_SM.PDF, 2019.

Rankin, A. M. and Wolff, E. W.: A year-long record of size-segregated aerosol composition at Halley, Antarctica, J. Geophys. Res. D Atmos., 108(D24), AAC 9-1-AAC 9-12, doi:10.1029/2003jd003993, 2003.

Ray, D., Kurková, R., Hovorková, I. and Klán, P.: Determination of the Specific Surface Area of Snow Using Ozonation of 1,1-Diphenylethylene, Environ. Sci. Technol., 45(23), 10061–10067, doi:10.1021/es202922k, 2011.

Rhodes, R. H., Yang, X., Wolff, E. W., McConnell, J. R. and Frey, M. M.: Sea ice as a source of sea salt aerosol to Greenland ice cores: A model-based study, Atmos. Chem. Phys., 17(15), 9417–9433, doi:10.5194/acp-17-9417-2017, 2017.

Richter, A., Wittrock, F., Eisinger, M. and Burrows, J. P.: GOME observations of tropospheric BrO in northern hemispheric spring and summer 1997, Geophys. Res. Lett., 25(14), 2683–2686, doi:10.1029/98GL52016, 1998.

Rodebush, W. H.: The freezing points of concentrated solutions and the free energy of solution of salts, J. Am. Chem. Soc., 40(8), 1204–1213, doi:10.1021/ja02241a008, 1918.

Rohatgi, P. K. and Adams, C. M.: Ice–Brine Dendritic Aggregate formed on Freezing of Aqueous Solutions, J. Glaciol., 6(47), 663–679, doi:Doi: 10.1017/s0022143000019936, 1967.

Roscoe, H. K., Brooks, B., Jackson, A. V, Smith, M. H., Walker, S. J., Obbard, R. W. and Wolff, E. W.: Frost flowers in the laboratory: Growth, characteristics, aerosol, and the underlying sea ice, J. Geophys. Res., 116(D12), D12301, doi:10.1029/2010JD015144, 2011.

Schenkmayerová, A., Bučko, M., Gemeiner, P., Treľová, D., Lacík, I., Chorvát, D., Ačai, P., Polakovič, M., Lipták, L., Rebroš, M., Rosenberg, M., Štefuca, V., Neděla, V. and Tihlaříková, E.: Physical and Bioengineering Properties of Polyvinyl Alcohol Lens-Shaped Particles Versus Spherical Polyelectrolyte Complex Microcapsules as Immobilisation Matrices for a Whole-Cell Baeyer–Villiger Monooxygenase, Appl. Biochem. Biotechnol., 174(5), 1834–1849, doi:10.1007/s12010-014-1174-x, 2014.

Schremb, M. and Tropea, C.: Solidification of supercooled water in the vicinity of a solid wall, Phys Rev E, 94(5–1), 52804, doi:10.1103/PhysRevE.94.052804, 2016.

Shibkov, A. A., Golovin, Y. I., Zheltov, M. A., Korolev, A. A. and Leonov, A. A.: Morphology diagram of nonequilibrium patterns of ice crystals growing in supercooled water, Phys. A Stat. Mech. its Appl., 319, 65–79, doi:https://doi.org/10.1016/S0378-4371(02)01517-0, 2003.

Simpson, W. R., Carlson, D., Hönninger, G., Douglas, T. A., Sturm, M., Perovich, D. and Platt, U.: First-year sea-ice contact predicts bromine monoxide (BrO) levels at Barrow, Alaska better than potential frost flower contact, Atmos. Chem. Phys., 7(3), 621–627, doi:10.5194/acp-7-621-2007, 2007.

Sundaramurthi, P., Shalaev, E. and Suryanarayanan, R.: “pH Swing” in Frozen Solutions-Consequence of Sequential Crystallization of Buffer Components, J. Phys. Chem. Lett., 1(1), 265–268, 2010.

Takenaka, N., Tanaka, M., Okitsu, K. and Bandow, H.: Rise in the pH of an unfrozen solution in ice due to the presence of

NaCl and promotion of decomposition of gallic acids owing to a change in the pH, J. Phys. Chem. A, 110(36), 10628–10632, 2006.

Vetráková, Ľ., Vykoukal, V. and Heger, D.: Comparing the acidities of aqueous, frozen, and freeze-dried phosphate buffers: Is there a "pH memory" effect?, Int. J. Pharm., 530(1–2), doi:10.1016/j.ijpharm.2017.08.005, 2017.

Vetráková, Ľ., Neděla, V., Runštuk, J. and Heger, D.: The morphology of ice and liquid brine in an environmental scanning electron microscope: a study of the freezing methods, Cryosph., 13(9), 2385–2405, doi:10.5194/tc-13-2385-2019, 2019.

Vetráková, Ľ., Neděla, V., Runštuk, J., Tihlaříková, E., Heger, D. and Shalaev, E.: Dynamical in-situ observation of the lyophilization and vacuum-drying processes of a model biopharmaceutical system by an environmental scanning electron microscope, Int. J. Pharm., 585, 119448, doi:10.1016/j.ijpharm.2020.119448, 2020.

Wagenbach, D., Ducroz, F., Mulvaney, R., Keck, L., Minikin, A., Legrand, M., Hall, J. S. and Wolff, E. W.: Sea-salt aerosol in coastal Antarctic regions, J. Geophys. Res. Atmos., 103(D9), 10961–10974, doi:10.1029/97JD01804, 1998.

Wettlaufer, J. S.: Directional solidification of salt water: deep and shallow cells, Eur. Lett., 19(4), 337–342, doi:10.1209/0295-5075/19/4/015, 1992.

Wexler, A.: Vapor pressure formulation for ice, J. Res. Natl. Bur. Stand., 81A(February), 5, doi:10.6028/jres.081A.003, 1977.

Wise, M. E., Baustian, K. J., Koop, T., Freedman, M. A., Jensen, E. J. and Tolbert, M. A.: Depositional ice nucleation onto crystalline hydrated NaCl particles: a new mechanism for ice formation in the troposphere, Atmos. Chem. Phys., 12(2), 1121–1134, doi:10.5194/acp-12-1121-2012, 2012.

Wolff, E. W., Rankin, A. M. and Röthlisberger, R.: An ice core indicator of Antarctic sea ice production?, Geophys. Res. Lett., 30(22), CLM 4-1-CLM 4-4, doi:10.1029/2003GL018454, 2003.

Workman, E. J. and Reynolds, S. E.: Electrical phenomena occurring during the freezing of dilute aqueous solutions and their possible relationship to thunderstorm electricity, Phys. Rev., 78(3), 254, doi:10.1103/PhysRev.78.254, 1950.

Yang, X., Pyle, J. A. and Cox, R. A.: Sea salt aerosol production and bromine release: Role of snow on sea ice, Geophys. Res. Lett., 35(16), 1–5, doi:10.1029/2008GL034536, 2008.

Yang, X., Neděla, V., Runštuk, J., Ondrušková, G., Krausko, J., Vetráková, Ľ. and Heger, D.: Evaporating brine from frost flowers with electron microscopy and implications for atmospheric chemistry and sea-salt aerosol formation, Atmos. Chem. Phys., 17(10), 6291–6303, doi:10.5194/acp-17-6291-2017, 2017.

Yang, X., Frey, M. M., Rhodes, R. H., Norris, S. J., Brooks, I. M., Anderson, P. S., Nishimura, K., Jones, A. E. and Wolff, E. W.: Sea salt aerosol production via sublimating wind-blown saline snow particles over sea ice: parameterizations and relevant microphysical mechanisms, Atmos. Chem. Phys., 19(13), 8407–8424, doi:10.5194/acp-19-8407-2019, 2019.

https://doi.org/10.5194/tc-2021-376
Preprint. Discussion started: 11 March 2022

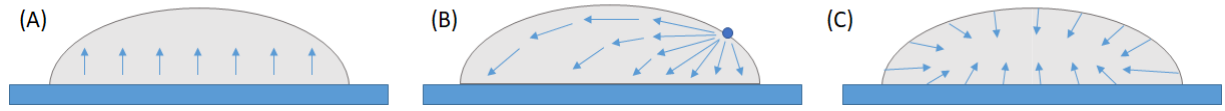

Figure 1: The directionalities of the three freezing methods: (A) Spontaneous freezing (non-seeded sample); (B) controlled ice nucleation (seeding); and (C) freezing in LN. The arrows show the expected directions of the progress of the ice crystal growth front.

740

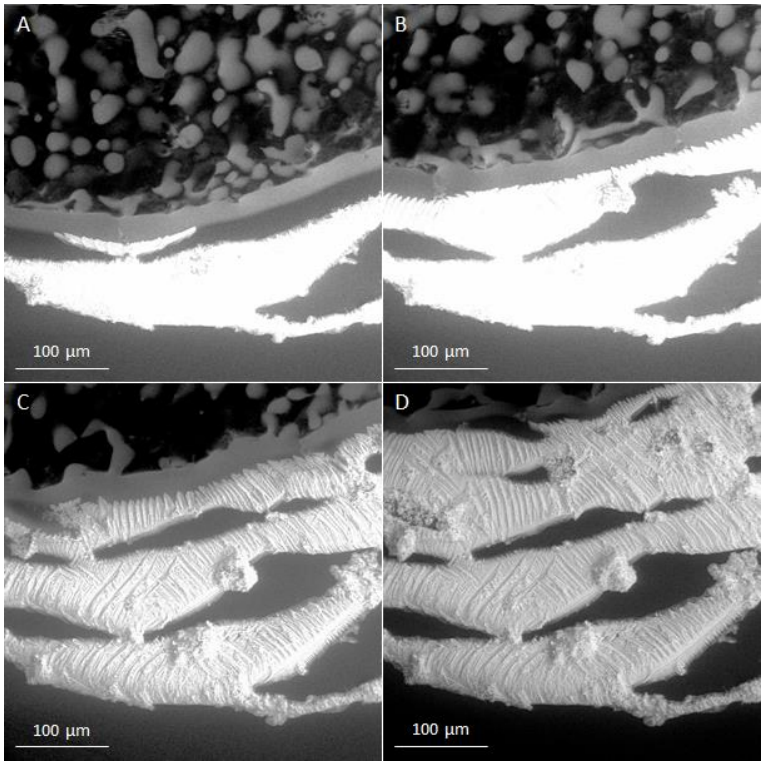

Figure 2: The sublimation process in the 0.5 M non-seeded sample at −20 °C. The images were recorded at the edge, within intervals of 10 s.

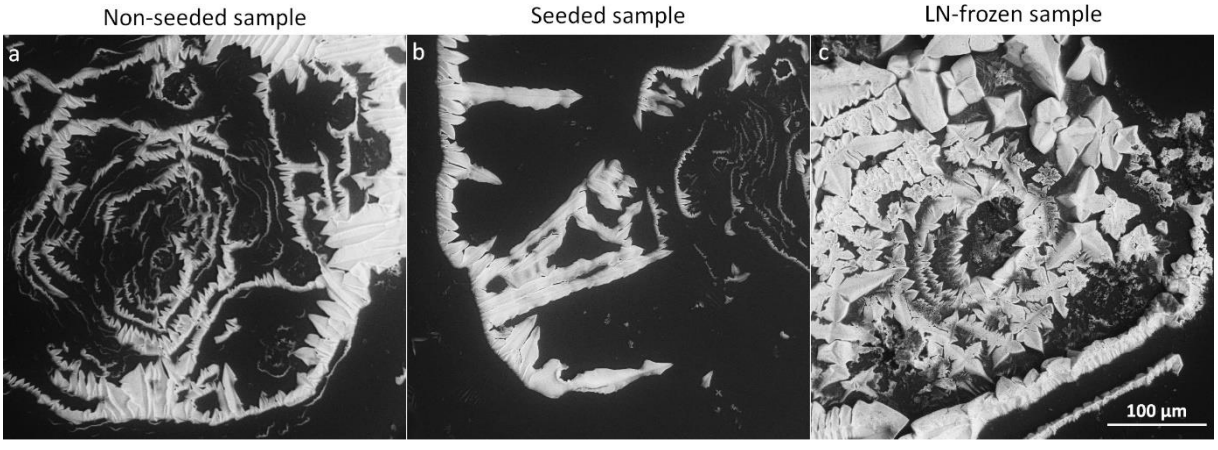

https://doi.org/10.5194/tc-2021-376
Preprint. Discussion started: 11 March 2022

The Cryosphere Discussions
Open Access
EGU

745 **Figure 3: The salt residua after the sublimation of the frozen samples prepared from 0.005 M CsCl via the indicated freezing methods. The samples sublimated at −20 °C (above the T_{eu}). The scale in panel *c* applies to all of the images.**

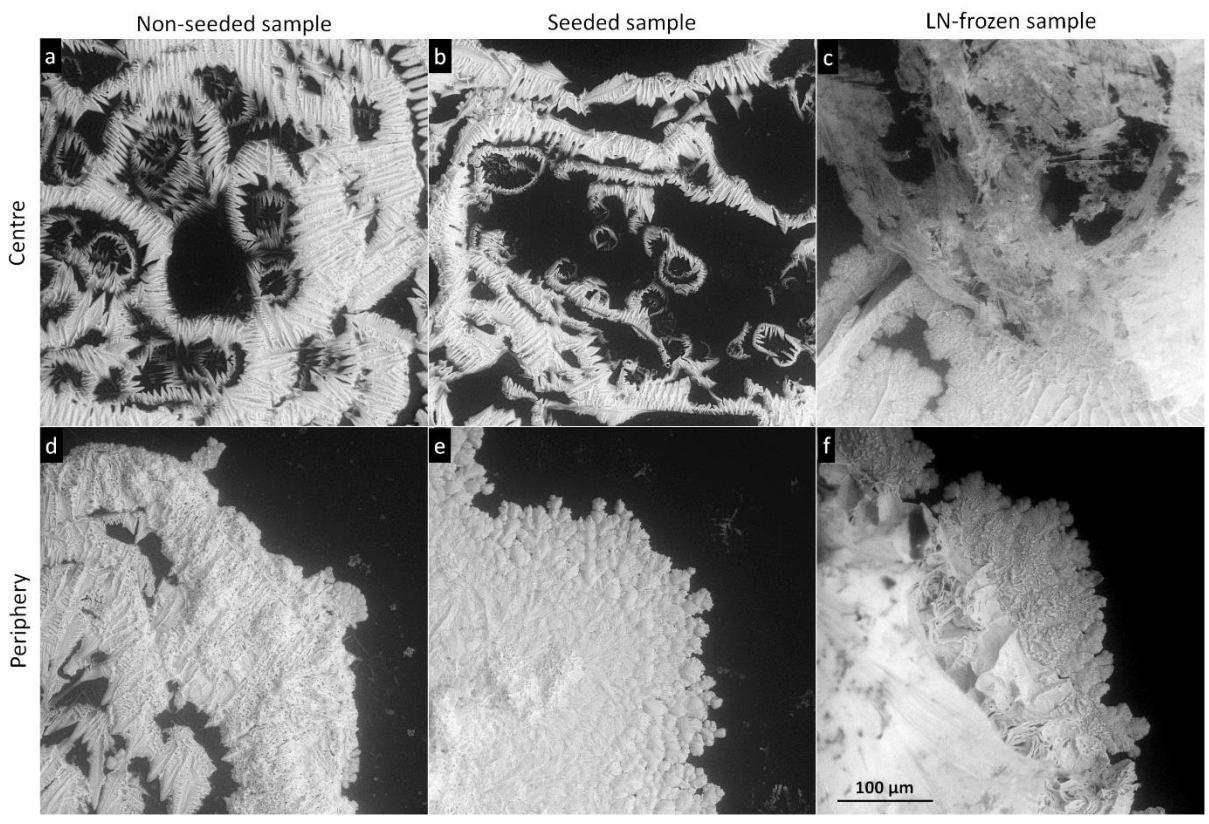

Figure 4: The salt residua after the sublimation of the frozen samples prepared from 0.05 M CsCl via the indicated freezing methods.
750 **The center and the periphery of the samples are displayed. The samples sublimated at −20 °C (above T_{eu}). The scale in panel f applies to all of the images.**

https://doi.org/10.5194/tc-2021-376
Preprint. Discussion started: 11 March 2022

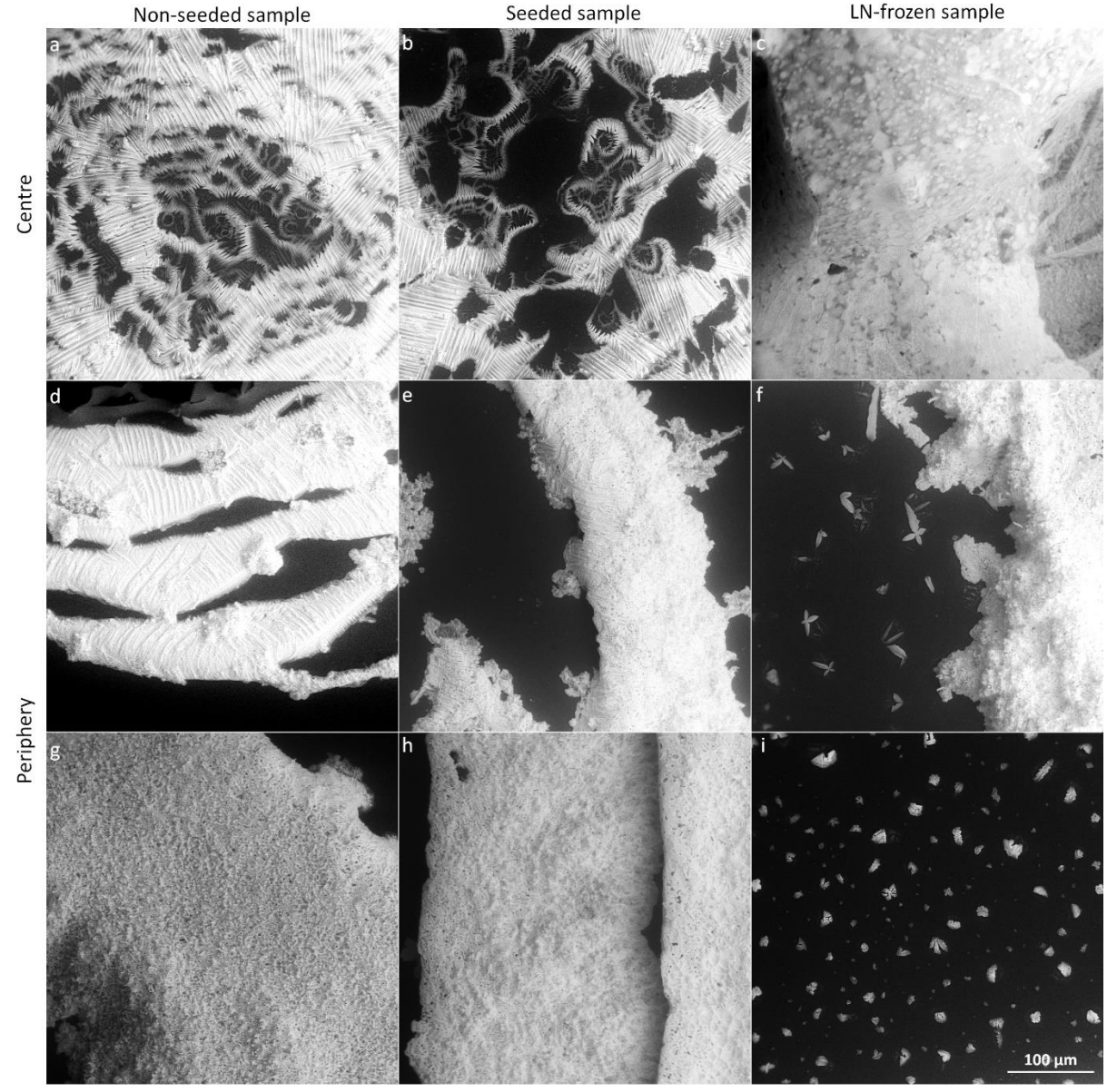

Figure 5: The salt residua after the sublimation of the frozen samples prepared from 0.5 M CsCl via the indicated freezing methods. The center and the periphery of the samples are displayed. The samples sublimated at −20 °C (above the T_{eu}). The scale in panel i applies to all of the images.

https://doi.org/10.5194/tc-2021-376
Preprint. Discussion started: 11 March 2022

Figure 6: A photograph of the cooling stage of the ESEM covered with the crystallized CsCl salt after the sublimation of the 0.5 M non-seeded sample at −20 °C. The diameter of the stage is about 6 mm. The pattern of the concentric circles is nicely visible.

https://doi.org/10.5194/tc-2021-376
Preprint. Discussion started: 11 March 2022

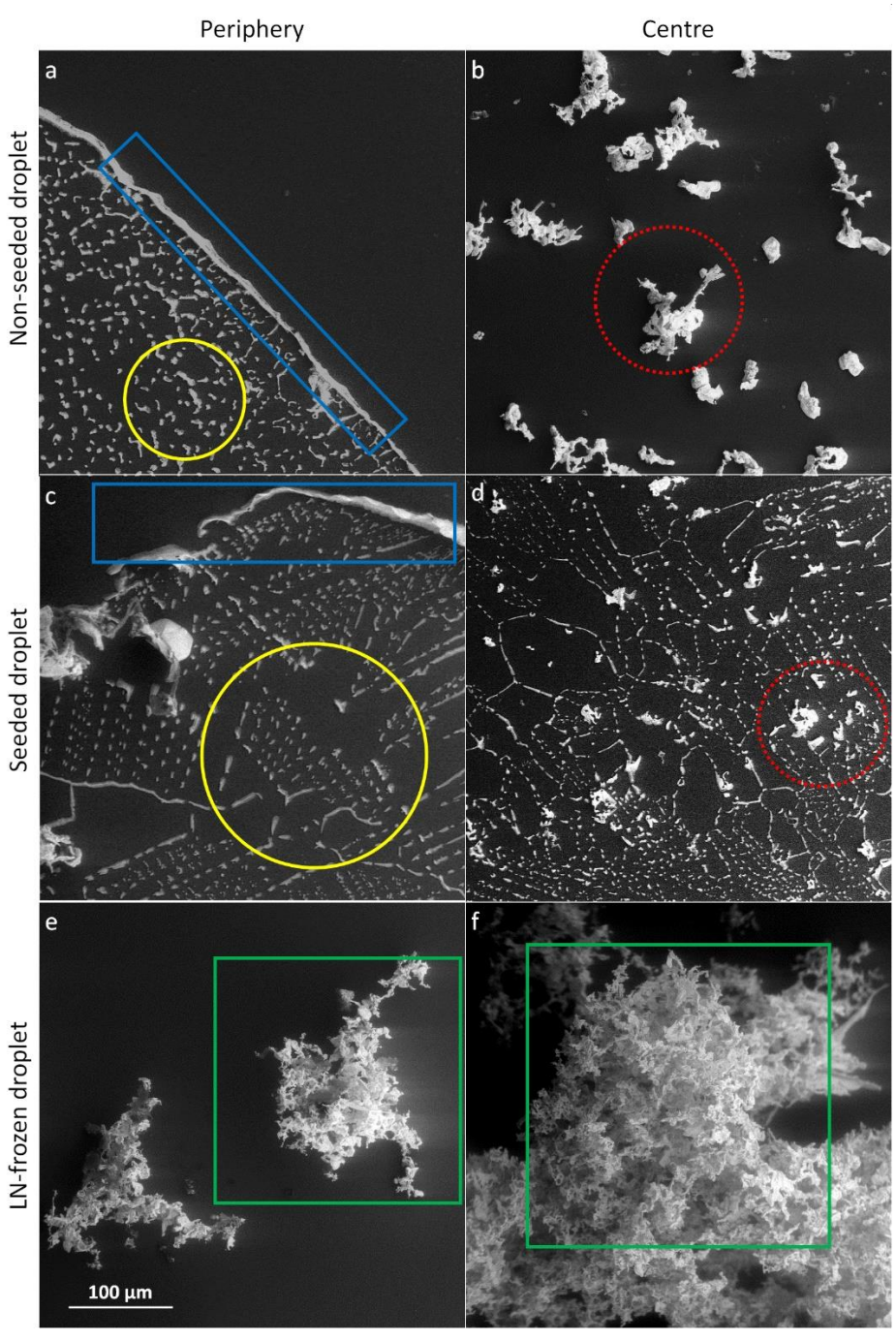

Figure 7: The salt residua after the sublimation of the frozen samples containing 0.005 M CsCl; the sublimation temperature was −25 °C (below the T_{eu}). Each row represents one freezing method, named on the left-hand side. The images in the left- and right-hand columns were taken at the periphery and close to the centre of the original sample, respectively. The scale in panel *e* applies to all the images. The examples of the salt rim (blue rectangles), fine salt particles (yellow circles), salt flakes (red dotted circles), and lichen-like tufts (green squares) are highlighted.

https://doi.org/10.5194/tc-2021-376
Preprint. Discussion started: 11 March 2022

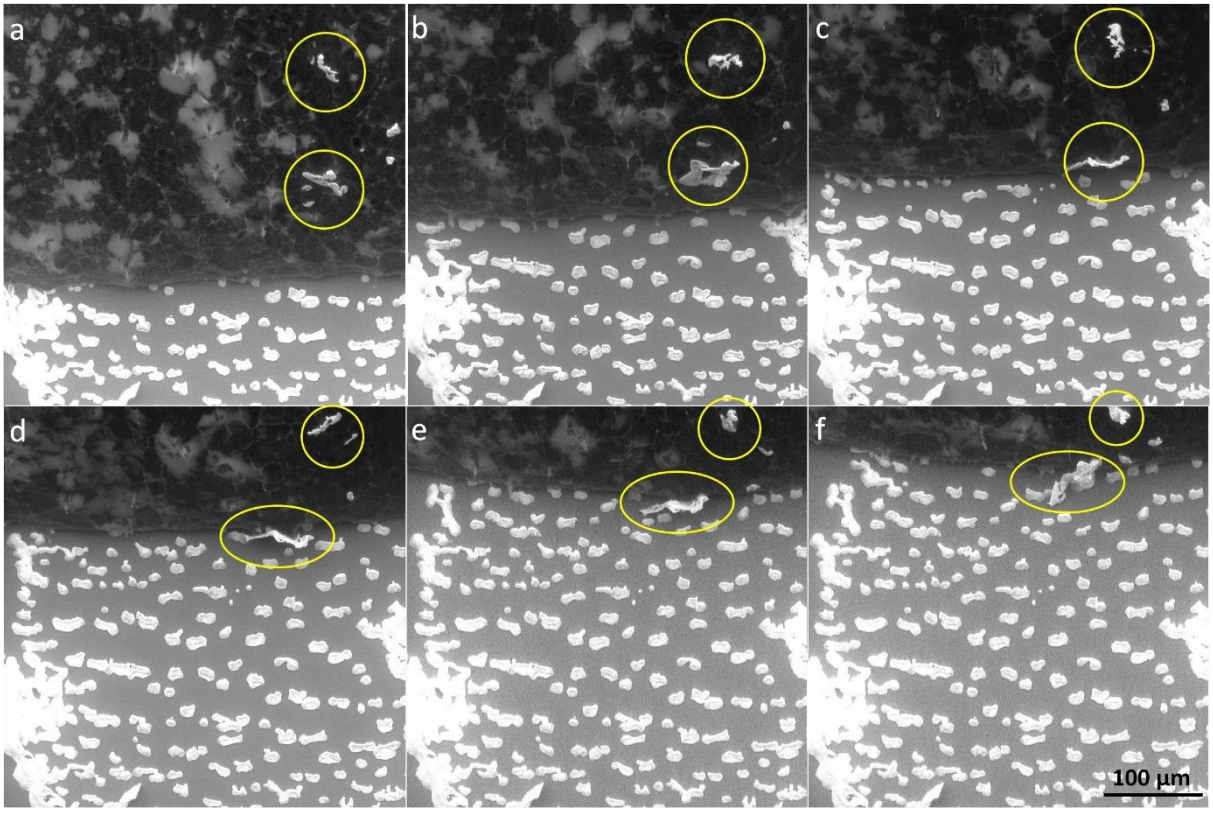

Figure 8. The retreating ice (black, upper part) in the 0.005 M non-seeded sample reveals salt particles (white) lying on the cooling stage (grey, lower part). The sublimation occurs at −25 °C. The encircled objects are the salt flakes on the ice surface.

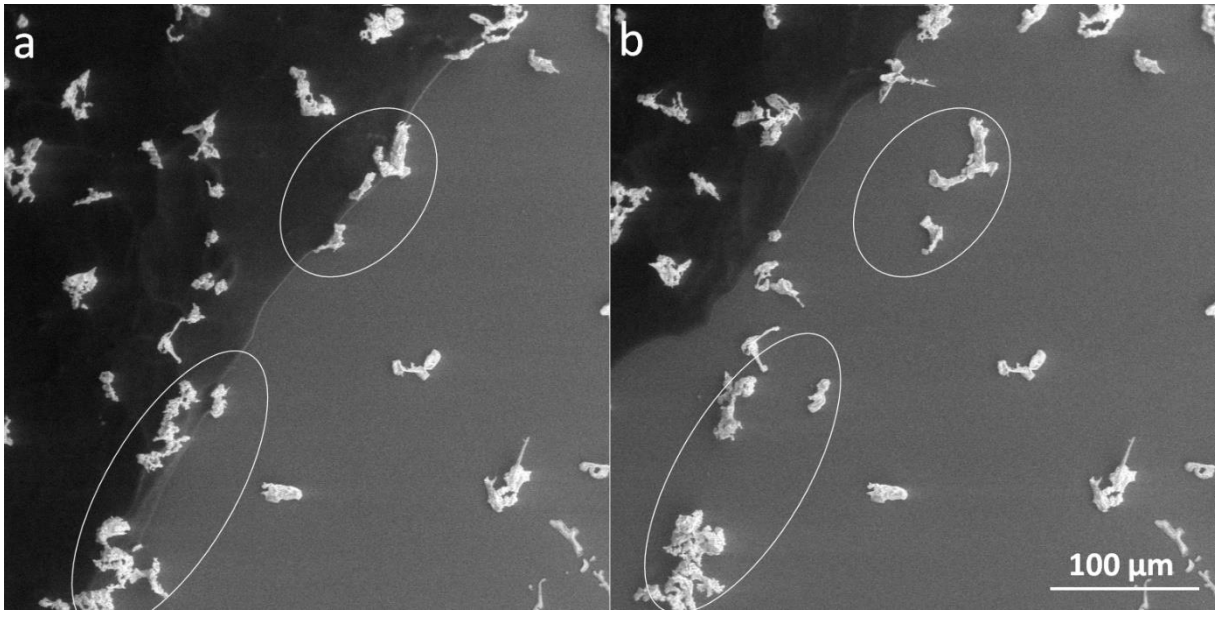

770

https://doi.org/10.5194/tc-2021-376
Preprint. Discussion started: 11 March 2022

The Cryosphere Discussions
Open Access
EGU

Figure 9: The salt flakes (white) falling down the surface of the retreating ice (black, left upper part) onto the cooling stage (grey, right part) in the 0.005 M seeded sample.

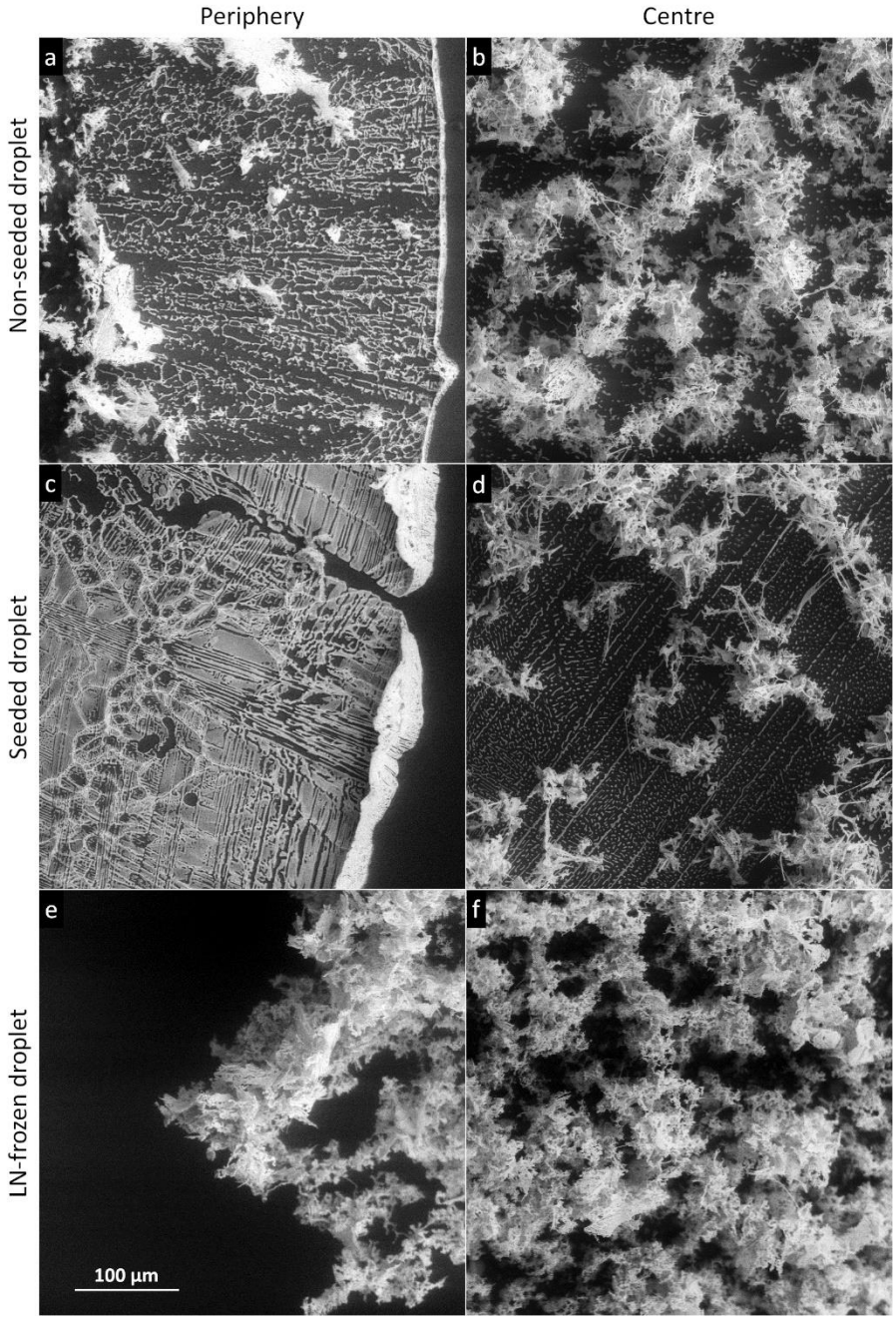

Figure 10: The salt residua after the sublimation of the frozen samples containing 0.05 M CsCl; the sublimation temperature was −25 °C (below the T_{eu}). Each row represents one freezing method, named on the left-hand side. The images in the left- and right-hand columns were taken at the periphery and close to the centre of the original sample, respectively. The scale in panel *e* applies to all of the images.

https://doi.org/10.5194/tc-2021-376
Preprint. Discussion started: 11 March 2022

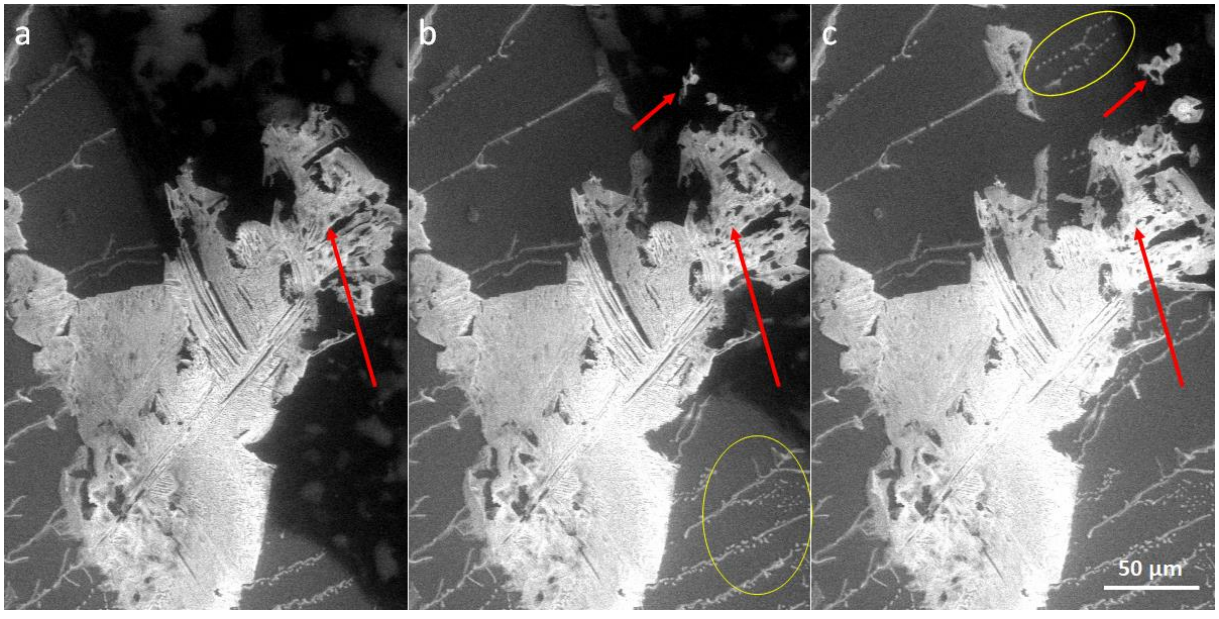

780 **Figure 11: The retreating ice (black) in the 0.05 M seeded sample reveals tiny salt particles (the white particles encircled in yellow) lying on the cooling stage (grey). These microparticles were most likely formed by the brine crystallizing at the bottom of the sample, in contact with the stage. Conversely, the larger salt flakes (pointed to by the red arrows), which emerge on the surface of the sample before falling down onto the stage, originate from the body and the surface of the sample.**

https://doi.org/10.5194/tc-2021-376
Preprint. Discussion started: 11 March 2022

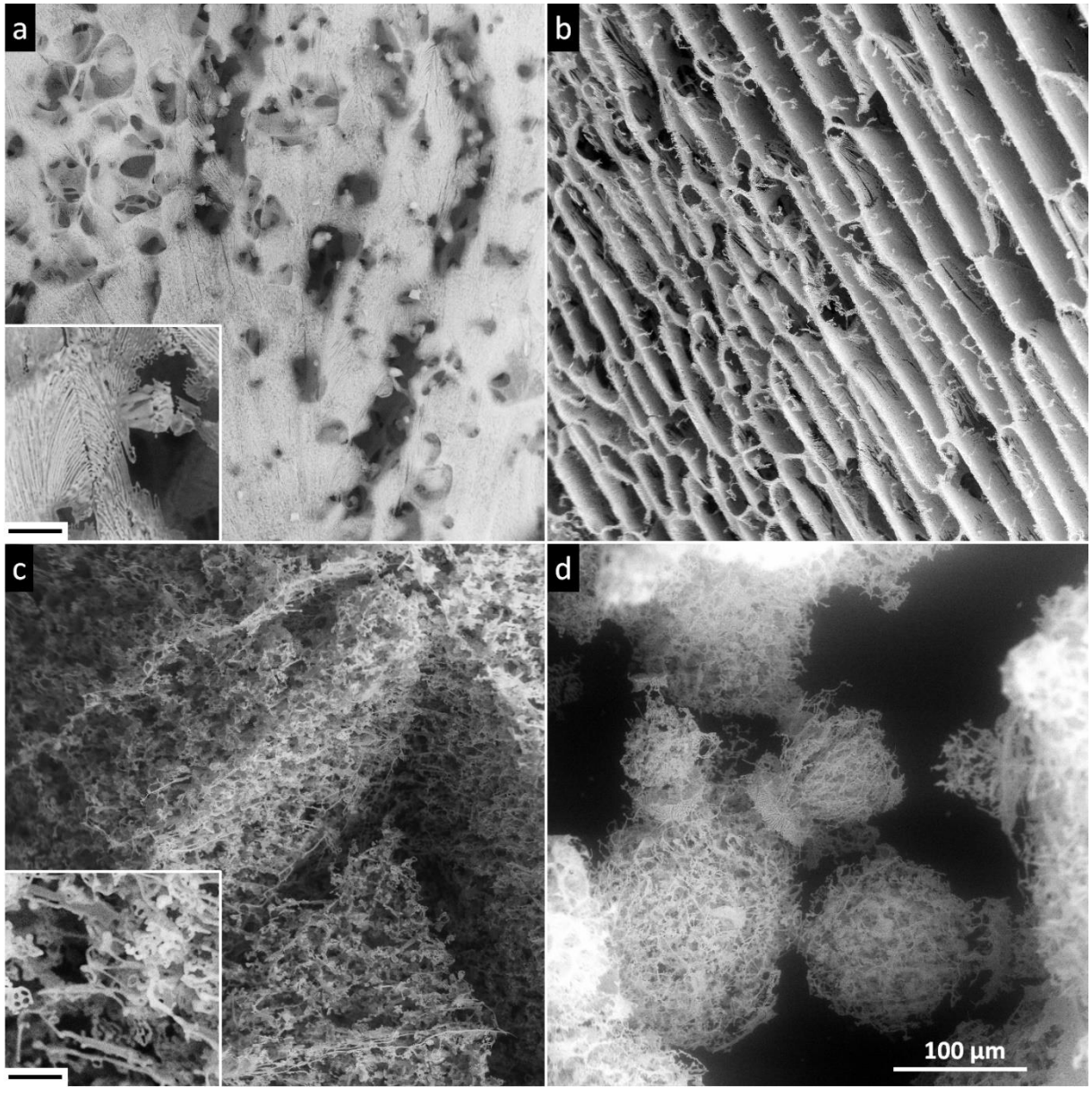

785 **Figure 12: The salt residua after the sublimation of the frozen samples containing 0.5 M CsCl: (a) a non-seeded droplet, (b) a seeded droplet, (c) an LN-frozen droplet, (d) LN-frozen microspheres. The samples sublimated at −25 °C (below the T_{eu}). The scale in panel *d* applies to all of the images. The corresponding morphologies are detailed in panels *a* and *c*, where the black bar represents 10 µm.**

https://doi.org/10.5194/tc-2021-376
Preprint. Discussion started: 11 March 2022

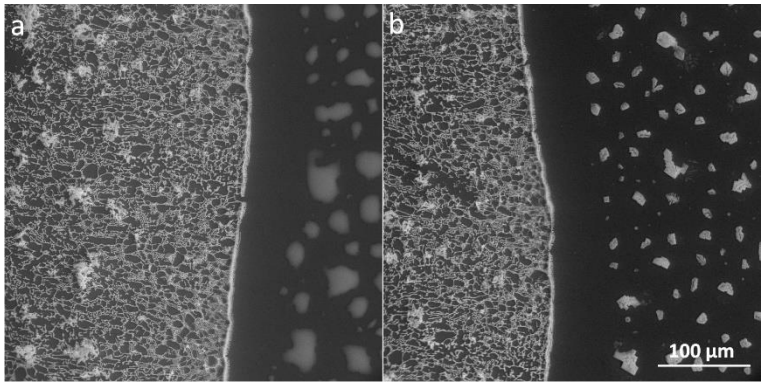

790 **Figure 13: The supercooled brine beyond the edge of the 0.05 M non-seeded sample (a) and the salt crystals formed via the eventual crystallization of the supercooled brine (b). The original frozen sample had been located in the left side of the panels a and b, its edge is represented by the broader white line (the salt rim).**

https://doi.org/10.5194/tc-2021-376
Preprint. Discussion started: 11 March 2022

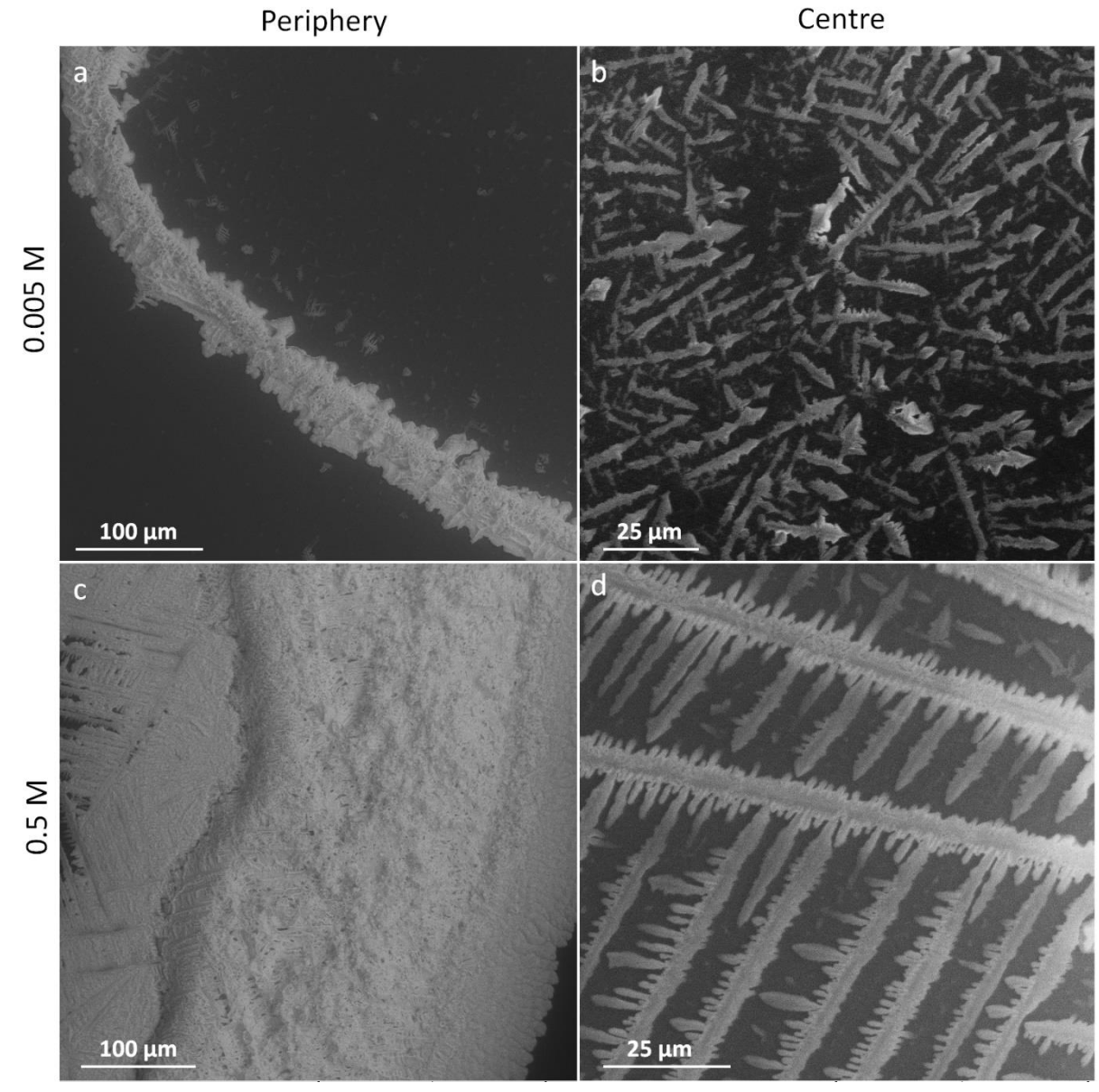

Figure 14: The structures of the CsCl salt residua after the evaporation of the 0.005 and 0.05 M liquid samples at 2 °C. We imaged spots close to the periphery and the centre of the original sample, respectively.

795

https://doi.org/10.5194/tc-2021-376
Preprint. Discussion started: 11 March 2022

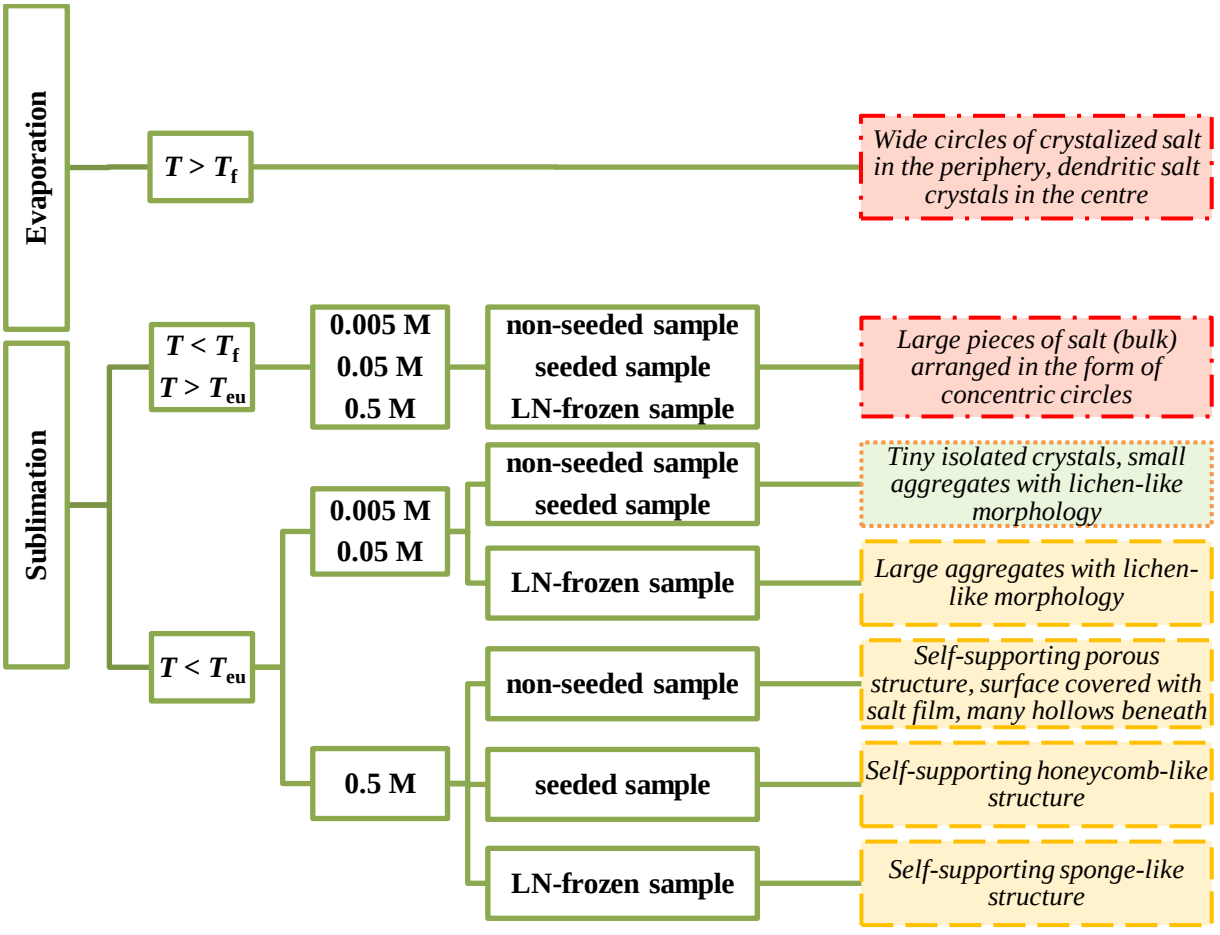

Figure 15: The structure of the salt residua after the sublimation of the ice, influenced by the sublimation temperature, salt concentration, and freezing method. According to their ability to be windblown and to become aerosols, the salt residua are categorized as follows: readily available (the green box with dotted border), potentially available after their mechanical breakdown (the yellow boxes with dashed borders), improbable (the red box with dash-dotted border).

https://doi.org/10.5194/tc-2021-376
Preprint. Discussion started: 11 March 2022

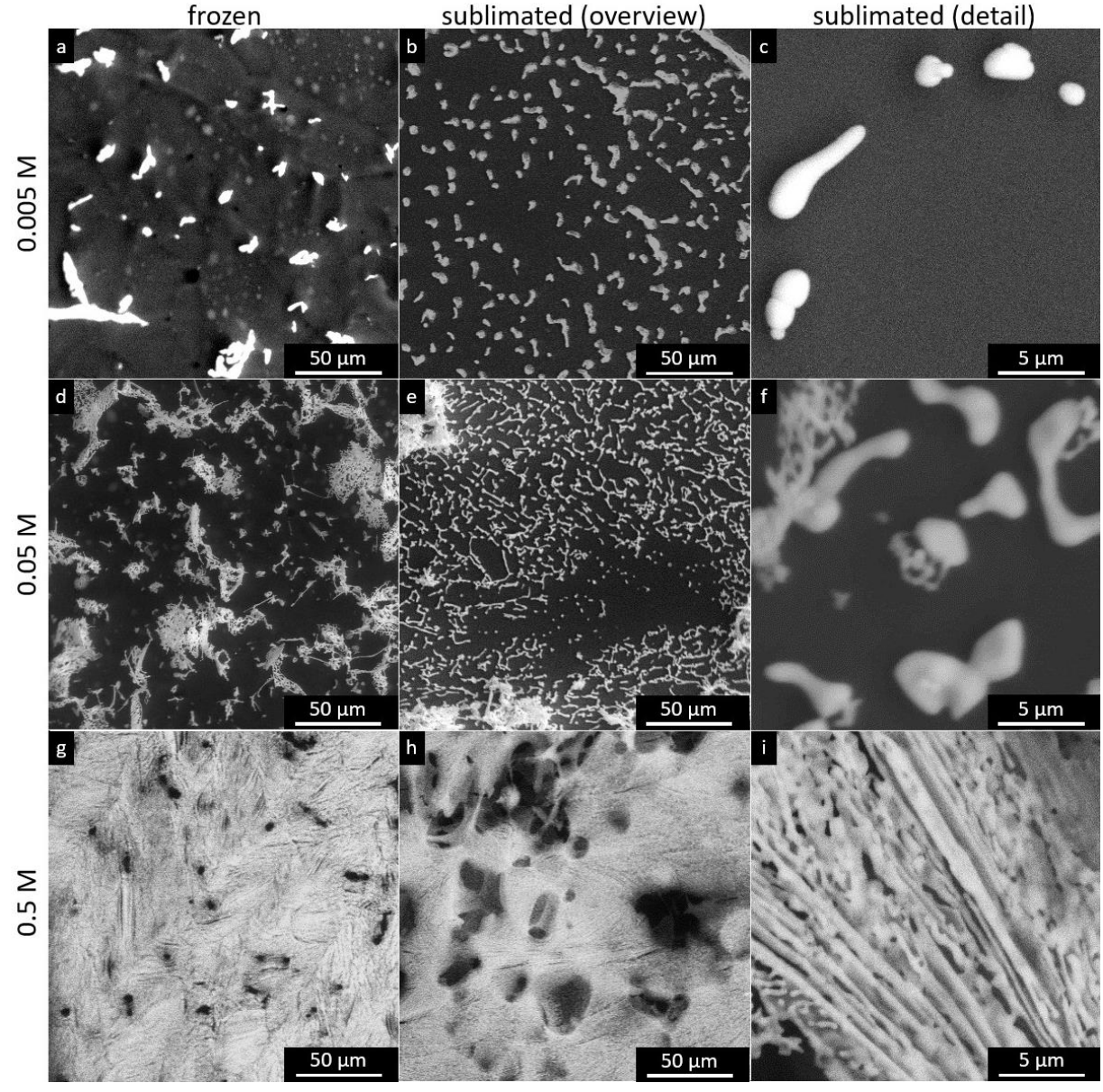

Figure 16. The structure of the frozen samples (before the sublimation) and the CsCl salt residua after the sublimation of the 0.005, 0.05, and 0.5 M spontaneously frozen samples at −25 °C, i.e. below $T_{eu.}$.

805

	0.005 M CsCl, non-seeded	0.005 M CsCl, seeded	0.05 M CsCl, non-seeded	0.05 M CsCl, seeded

https://doi.org/10.5194/tc-2021-376
Preprint. Discussion started: 11 March 2022

The Cryosphere Discussions
Open Access
EGU

Surface density of salt particles / mm^{-2}	3405 ± 3033	11934 ± 6350	39200 ± 25032	59625 ± 11885
Volume density of salt particles / mm^{-3}	6300 ± 5613	22081 ± 11748	72528 ± 46314	110319 ± 21989

Table 1. The calculated surface and volume densities (mm^{-3}) with sample standard deviations under different conditions. The method of the calculation is described in SI (Text S1, Table S1).

810

Concentration	Freezing method	**The occurrence of residual salt particles according to their sizes**				
		1 to 10 µm	10 to 100 µm	100 to 200 µm	200 to 400 µm	> 400 µm
0.005 M	Non-seeded	***	***			
	Seeded	***	**			
	LN-frozen			**	*	***
0.05 M	Non-seeded	***	***	**	*	
	Seeded	***	***	***	***	
	LN-frozen			*	**	***
0.5 M	Non-seeded					***
	Seeded					***
	LN-frozen					***

Table 2: The distribution of the sizes of the residual salt particles in the samples sublimated at −25 °C. The occurrence of the particles according to their sizes is expressed as follows: * often; ** occasionally; * seldom.**

815